SPIE.SPOTLIGHT

Arrayed Waveguide Gratings

Dana Seyringer

Arrayed Waveguide Gratings

by Dana Seyringer

doi: http://dx.doi.org/10.1117/3.2242852
PDF ISBN: 9781510603592
epub ISBN: 9781510603608
mobi ISBN: 9781510603615

Published by

SPIE Press
P.O. Box 10
Bellingham, Washington 98227-0010 USA
Phone: +1 360.676.3290
Fax: +1 360.647.1445
Email: Books@spie.org
Web: http://spie.org

Spotlight vol. SL16
Last updated 2 June 2016

SPIE.

Table of Contents

SPIE Spotlight Series

Welcome to SPIE Spotlight eBooks! This series of tutorials is designed to educate readers about a wide range of topics in optics and photonics. I like to think that these books address subjects that are too broad for journal articles but too concise for textbooks. We hope you enjoy this eBook, and we encourage you to submit your ideas for future Spotlights online.

Robert D. Fiete, *Series Editor*
Harris Corp.

Editorial Board

1 Introduction

On average, data traffic in the internet grows by 40% each year. This growth, and, in particular, the rapidly increasing interest in videos on demand, in multiplayer online games, and in selling music and software over the World Wide Web, naturally places huge demands on the speed of data transfer. When sending data using conventional electric data transfer, only one electric signal can be transferred per cable. Using optical data transmission, it is possible to send several optical signals simultaneously in one glass fiber without them interfering with one another. This technology, known as wavelength division multiplexing (WDM), is of considerable importance and has one major advantage, namely that even without new infrastructure and using as few as two colors, the transmission capacity of the glass fiber cable can be doubled. The more wavelengths used, therefore, means more data can be transferred. This technology allows an enormous amount of data to be transferred through just one glass fiber 10 times thinner than a human hair. Particularly in large cities where the laying of new glass fiber cables involves considerable cost and difficulty, WDM technology has revolutionized data transfer.

Passive optical components such as optical multiplexers (MUX)/demultiplexers (DeMUX) play an important role in this rapidly developing technology. Optical MUX are used to combine the different optical signals that carry the data on one optical fiber. Once the data have been transmitted over long distances, optical DeMUX then split the optical signals back into separate wavelengths.

This Spotlight aims to provide an overview of the life cycle of optical MUX/DeMUX based on arrayed waveguide gratings (AWGs), from the principle, design, and simulation through evaluation and technological verification. The main topics covered are as follows:

- **Principle:** The basic principle of AWG operation is described.
- **Design:** The procedure of designing an AWG using the "AWG-Parameters" tool is presented. This tool was used in various AWG designs and is experimentally well verified.
- **Simulation:** Different commercially available photonics tools are used to simulate the resulting AWG layouts. The suitability of these tools, as well as their advantages and disadvantages, are discussed.
- **Evaluation:** In order to evaluate the performance of the AWGs, 19 different transmission parameters were defined. These parameters were calculated by the "AWG-Analyzer" software tool, which is described in detail.
- **Fabrication:** Fabrication is a critical phase in the AWG life cycle, as AWGs are very sensitive to fabrication imperfections. It is shown that when designing AWGs, the influence of possible technological imperfections and process variations must be considered in the early stages of the design process.

- **Optimization:** There is great scope for flexibility when designing AWGs. However, the standard design approach is not always sufficient to reach the required AWG specifications, and in such cases it may be necessary to look for new solutions. Some new ideas are introduced here.
- **AWG designs:** Special designs, such as colorless AWGs, coarse wavelength division multiplexing (CWDM) flat-top AWGs or narrow-channel-spacing, high-channel-count 256-channel 25-GHz AWGs, and 128-channel 10-GHz AWGs, are described in this Spotlight.

2 Wavelength Division Multiplexing

WDM is the process by which multiple wavelengths carrying data are simultaneously combined in a single optical fiber and then separated again at the receiving end. During data transfer, each frequency window remains a separate data signal at any bit rate with any protocol, unaffected by other signals on the fiber.[1]

2.1 WDM system

The simple point-to-point optical system consists of transponders (transmitters and receivers), amplifiers, and attenuators (Fig. 1). These components, conforming to International Telecommunication Union (ITU) channel standards, also known as the ITU frequency grid, allow a WDM system to implement optical solutions throughout the network, i.e., to interface with the networks' nonoptical part.

An electro-optic transmitter generates optical bits from electrical bits (coming from the nonoptical part of the network). The most common devices used as light sources in optical transmitters are light emitting diodes (LEDs) for short-distance transmissions and lasers for long-distance transmissions. The transmitted optical signal is then transported via optical fiber to the receiver. The optical receiver converts the modulated light coming from the optical fiber back into a replica of the original electrical signal applied to the transmitter, thus allowing it to be transmitted again through the nonoptical part of the network. The photodetector receiving this modulated light is usually a photodiode. If the optical signal is intended to travel long distances, amplification of the signal is required at regular intervals.

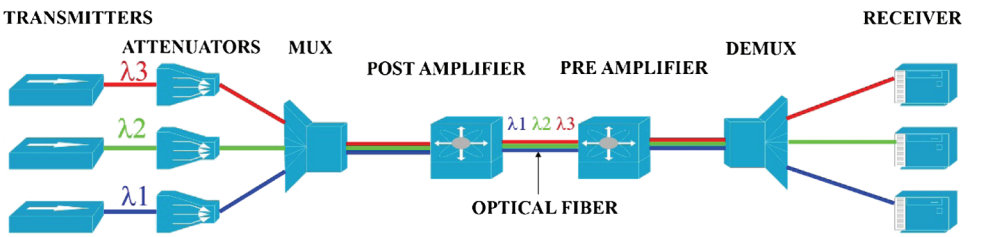

Figure 1 WDM system.

The optical amplifier provides a cost-efficient method of amplifying optical signals without converting them into electrical signals.

A point-to-point optical system increases the bandwidth, but has no influence on the network capacity. In order to increase the capacity of transmitted data, multiple optical signals with different wavelengths can be combined together on a single fiber simply by adding optical MUX. On the receiving end, the data must be split back into separate wavelengths by adding optical DeMUX (Fig. 1). Each optical signal carrying information at a different wavelength (also called the transmitting channel) will then need its own transmitter to send the signal down the fiber and its own light detector to convert the signal back into useful information.

2.2 Different WDM systems

There are three types of WDM systems, which are classified according to the number of transmitting channels and the channel spacing (as defined by the ITU frequency grid, Fig. 2):

- Coarse wavelength division multiplexing (CWDM) uses a wide spectrum and typically accommodates up to eight transmitting channels. While such wide spacing of channels (2500 GHz) allows the use of moderately priced optics, it also limits capacity. Therefore, CWDM is typically used for lower-cost, lower-capacity, shorter-distance applications where cost is paramount in the decision-making process.
- Dense wavelength division multiplexing (DWDM) systems squeeze 16 or more transmitting channels (usually with 100- or 50-GHz channel spacing) into a narrow spectrum window very near the 1550-nm local attenuation minimum of the glass fiber. Decreasing channel spacing requires the use of more precise and costly optics, but allows for significantly more scalability. Typical DWDM systems provide up to 64 transmitting channels with a channel separation down to 50 GHz. Optical systems operating with <16 channels, e.g., 2, 4, or 8, and having channel spacing of 100 GHz or more, e.g., 200 GHz, are usually referred to as WDM systems.
- High dense wavelength division multiplexing (HDWDM) and very high dense wavelength division multiplexing (VHDWDM), also called ultra-DWDM, systems have been developed to meet the growing capacity demands by increasing the transmission channel counts as far as possible (starting from 128), i.e., by decreasing channel spacing down to 25 GHz, 12.5 GHz, or even less.

2.3 Flex-grid ITU standards

The frequency grid for DWDM applications described above is defined by the ITU-T G.694.1 recommendation.[2] It is anchored at 193.1 GHz and supports fixed

L-Band				C-Band				S-Band			
100 GHz		50 GHz		100 GHz		50 GHz		100 GHz		50 GHz	
THz	nm	THz	nm	THz	nm	THz	nm	THz	nm	THz	nm
186.00	1611.79	186.05	1611.35	191.00	1569.59	191.05	1569.18	196.00	1529.55	196.05	1529.16
186.10	1610.92	186.15	1610.49	191.10	1568.77	191.15	1568.36	196.10	1528.77	196.15	1528.38
186.20	1610.06	186.25	1609.62	191.20	1567.95	191.25	1567.54	196.20	1527.99	196.25	1527.60
186.30	1609.19	186.35	1608.76	191.30	1567.13	191.35	1566.72	196.30	1527.22	196.35	1526.83
186.40	1608.33	186.45	1607.90	191.40	1566.31	191.45	1565.90	196.40	1526.44	196.45	1526.05
186.50	1607.47	186.55	1607.04	191.50	1565.50	191.55	1565.09	196.50	1525.66	196.55	1525.27
186.60	1606.60	186.65	1606.17	191.60	1564.68	191.65	1564.27	196.60	1524.89	196.65	1524.50
186.70	1605.74	186.75	1605.31	191.70	1563.86	191.75	1563.45	196.70	1524.11	196.75	1523.72
186.80	1604.88	186.85	1604.46	191.80	1563.05	191.85	1562.64	196.80	1523.34	196.85	1522.95
186.90	1604.03	186.95	1603.60	191.90	1562.23	191.95	1561.83	196.90	1522.56	196.95	1522.18
187.00	1603.17	187.05	1602.74	192.00	1561.42	192.05	1561.01	197.00	1521.79	197.05	1521.40
187.10	1602.31	187.15	1601.88	192.10	1560.61	192.15	1560.20	197.10	1521.02	197.15	1520.63
187.20	1601.46	187.25	1601.03	192.20	1559.79	192.25	1559.39	197.20	1520.25	197.25	1519.86
187.30	1600.60	187.35	1600.17	192.30	1558.98	192.35	1558.58	197.30	1519.48	197.35	1519.09
187.40	1599.75	187.45	1599.32	192.40	1558.17	192.45	1557.77	197.40	1518.71	197.45	1518.32
187.50	1598.89	187.55	1598.47	192.50	1557.36	192.55	1556.96	197.50	1517.94	197.55	1517.55
187.60	1598.04	187.65	1597.62	192.60	1556.55	192.65	1556.15	197.60	1517.17	197.65	1516.78
187.70	1597.19	187.75	1596.76	192.70	1555.75	192.75	1555.34	197.70	1516.40	197.75	1516.02
187.80	1596.34	187.85	1595.91	192.80	1554.94	192.85	1554.54	197.80	1515.63	197.85	1515.25
187.90	1595.49	187.95	1595.06	192.90	1554.13	192.95	1553.73	197.90	1514.87	197.95	1514.49
188.00	1594.64	188.05	1594.22	193.00	1553.33	193.05	1552.93	198.00	1514.10	198.05	1513.72
188.10	1593.79	188.15	1593.37	193.10	1552.52	193.15	1552.12	198.10	1513.34	198.15	1512.96
188.20	1592.95	188.25	1592.52	193.20	1551.72	193.25	1551.32	198.20	1512.58	198.25	1512.19
188.30	1592.10	188.35	1591.68	193.30	1550.92	193.35	1550.52	198.30	1511.81	198.35	1511.43
188.40	1591.26	188.45	1590.83	193.40	1550.12	193.45	1549.72	198.40	1511.05	198.45	1510.67
188.50	1590.41	188.55	1589.99	193.50	1549.32	193.55	1548.91	198.50	1510.29	198.55	1509.91
188.60	1589.57	188.65	1589.15	193.60	1548.51	193.65	1548.11	198.60	1509.53	198.65	1509.15
188.70	1588.73	188.75	1588.30	193.70	1547.72	193.75	1547.32	198.70	1508.77	198.75	1508.39
188.80	1587.88	188.85	1587.46	193.80	1546.92	193.85	1546.52	198.80	1508.01	198.85	1507.63
188.90	1587.04	188.95	1586.62	193.90	1546.12	193.95	1545.72	198.90	1507.25	198.95	1506.87
189.00	1586.20	189.05	1585.78	194.00	1545.32	194.05	1544.92	199.00	1506.49	199.05	1506.12
189.10	1585.36	189.15	1584.95	194.10	1544.53	194.15	1544.13	199.10	1505.74	199.15	1505.36
189.20	1584.53	189.25	1584.11	194.20	1543.73	194.25	1543.33	199.20	1504.98	199.25	1504.60
189.30	1583.69	189.35	1583.27	194.30	1542.94	194.35	1542.54	199.30	1504.23	199.35	1503.85
189.40	1582.85	189.45	1582.44	194.40	1542.14	194.45	1541.75	199.40	1503.47	199.45	1503.10
189.50	1582.02	189.55	1581.60	194.50	1541.35	194.55	1540.95	199.50	1502.72	199.55	1502.34
189.60	1581.18	189.65	1580.77	194.60	1540.56	194.65	1540.16	199.60	1501.97	199.65	1501.59
189.70	1580.35	189.75	1579.93	194.70	1539.77	194.75	1539.37	199.70	1501.21	199.75	1500.84
189.80	1579.52	189.85	1579.10	194.80	1538.98	194.85	1538.58	199.80	1500.46	199.85	1500.09
189.90	1578.69	189.95	1578.27	194.90	1538.19	194.95	1537.79	199.90	1499.71	199.95	1499.34
190.00	1577.86	190.05	1577.44	195.00	1537.40	195.05	1537.00	200.00	1498.96	200.05	1498.59
190.10	1577.03	190.15	1576.61	195.10	1536.61	195.15	1536.22	200.10	1498.21	200.15	1497.84
190.20	1576.20	190.25	1575.78	195.20	1535.82	195.25	1535.43	200.20	1497.46	200.25	1497.09
190.30	1575.37	190.35	1574.95	195.30	1535.04	195.35	1534.64	200.30	1496.72	200.35	1496.34
190.40	1574.54	190.45	1574.13	195.40	1534.25	195.45	1533.86	200.40	1495.97	200.45	1495.60
190.50	1573.71	190.55	1573.30	195.50	1533.47	195.55	1533.07	200.50	1495.22	200.55	1494.85
190.60	1572.89	190.65	1572.48	195.60	1532.68	195.65	1532.29	200.60	1494.48	200.65	1494.11
190.70	1572.06	190.75	1571.65	195.70	1531.90	195.75	1531.51	200.70	1493.73	200.75	1493.36
190.80	1571.24	190.85	1570.83	195.80	1531.12	195.85	1530.72	200.80	1492.99	200.85	1492.62
190.90	1570.42	190.95	1570.01	195.90	1530.33	195.95	1529.94	200.90	1492.25	200.95	1491.88

Figure 2 ITU grid.

channel spacings of 12.5 up to 100 GHz and wider (in integer multiples of 100 GHz).

With the internet and the many different internet services (such as video conferencing, cloud services, and video streaming) causing traffic demands to grow

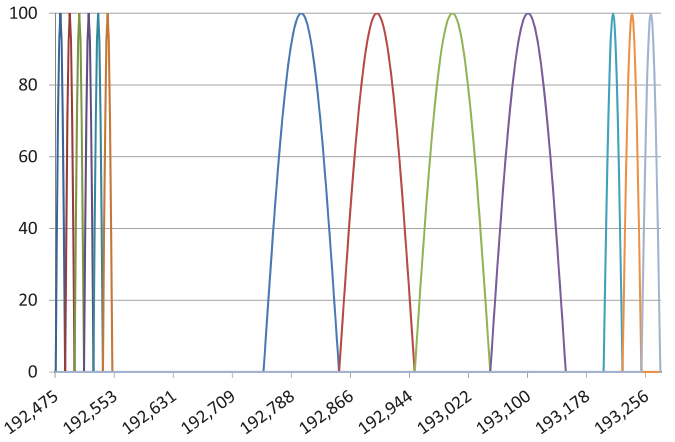

Figure 3 Three different groups of channels with channel spacings of 12.5, 100, and 25 GHz, which could belong to three different operators using different technologies but sharing the same fiber.

exponentially, leading to a massive rise in traffic in the core optical networks, network operators must keep increasing their optical network capacity. However, the fixed-grid technology is no longer flexible enough to handle such rapidly changing channel requirements. Therefore, the ITU-T G.694.1 recommendation has defined a new, flexible DWDM grid standard (so-called flex grid[2]) for WDM applications. This flexible spectral grid has the same nominal central frequency as in the standard DWDM grids, namely 193.1 GHz, but the central frequency granularity is 6.25 GHz, and the slot-width granularity is 12.5 GHz. The great advantage of the flexible grid is that the slots need not be 12.5 GHz wide; rather, they may be any integer multiple of 12.5 GHz. They can be joined together to form arbitrary-sized blocks of spectra having any integer multiples of 12.5 GHz, which allow for 25, 50, 100 GHz, and beyond. Even slots with 37.5 GHz (3×12.5 GHz) are possible, which was not the case with standard WDM fixed grids.

Additional flexibility is offered by the fact that different slot widths may be combined, allowing for optimization of the bandwidth of the particular bit rate and modulation scheme of the individual channels. The example in Fig. 3 shows three different groups of channels with a channel spacing of 12.5, 100, and 25 GHz, which could belong to three different operators using different technologies but sharing the same fiber.

2.4 Multiplexing/demultiplexing approaches

Optical MUX/DeMUX are the key components in any type of WDM system. Their task is to multiplex optical signals onto a single fiber and then to separate them according to the wavelengths on the receiving end of the optical network.

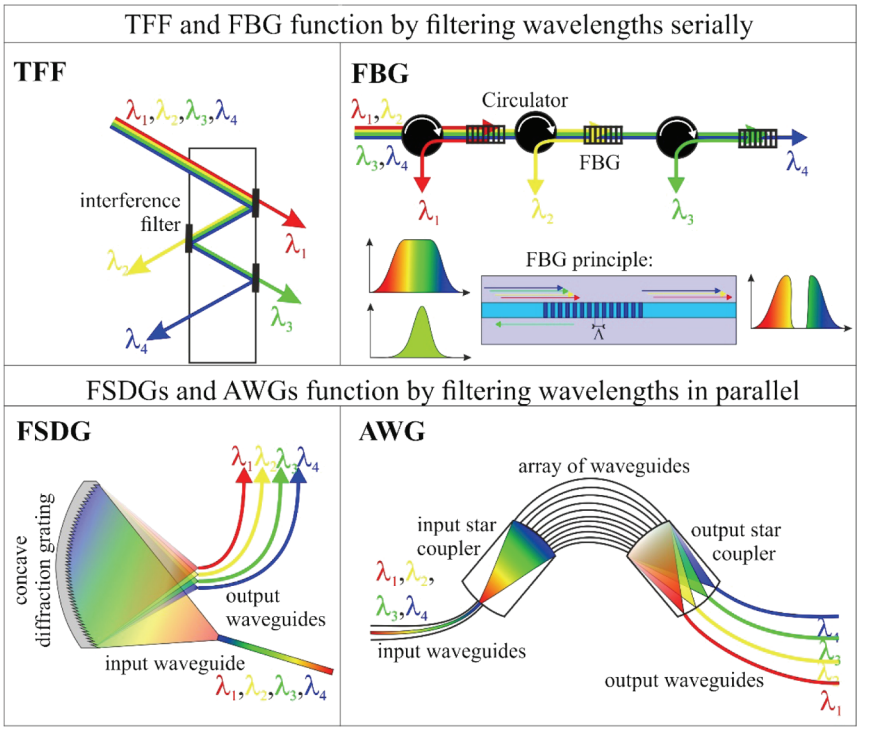

Figure 4 Different demultiplexing approaches.

There are four basic MUX/DeMUX approaches: thin film filter (TFF), fiber Bragg grating (FBG), AWG, and free-space diffraction grating (FSDG).[3]

TFFs and FBGs were the first of those used in WDM systems when channel counts were low. Although they use different physical mechanisms, they both function by filtering wavelengths serially, whereby individual elements are used to MUX (or DeMUX) wavelengths on a one-by-one basis.[4] In contrast to TFFs and FBGs, AWGs and FSDGs use a parallel approach that is more conducive to high-channel-count applications (Fig. 4).

TFFs use a concatenated set of individual interference filters, each of which has multiple dielectric coatings that pass a single wavelength and reflect all others (Fig. 4—TFF). TFFs work well for low channel counts but have limitations at higher channel counts (typically >16) due to size and accumulated insertion losses.[5,6]

FBGs rely on a grating formed in the fiber core, which reflects a single wavelength but transmits all other wavelengths (Fig. 4—FBG). Each FBG is designed with a different grating period Λ to MUX or DeMUX a single wavelength in the system. The reflected wavelength is demultiplexed from the system fiber using an optical circulator. As is the case for TFFs, the serial process restricts the practical channel count due to size, accumulated insertion losses, and the cost of individual piece parts.[7]

AWGs consist of input/output (I/O) waveguides, two star couplers, and an array of waveguides with a certain length difference between them that causes a corresponding phase shift among diffracted beams, providing the imaging and dispersive properties required for demultiplexing.[8] The positioning of the output waveguides at the focal points in the image plane of the output star coupler allows the spatial separation of the different wavelengths (Fig. 4—AWG).

FSDGs work on a principle similar to that of the AWGs. The gratings are termed free-space gratings because the phase difference between diffracted beams is generated in free space rather than in dispersion media, such as waveguides.[9,10] The basic elements of an FSDG are the input and output fibers, micro-optics array, collimating lenses, and a finely ruled or etched diffraction grating that serves as the dispersion engine to separate wavelengths into individual output fibers. When a polychromatic light beam impinges on a diffraction grating, each wavelength is diffracted and directed to a different point in space. A fiber is placed at the focal point of each wavelength. In order to focus the different wavelengths, a lens system or a concave diffraction grating may be used (Fig. 4—FSDG).

3 Arrayed Waveguide Gratings

AWGs were proposed and first reported by Smit.[11] The first devices operating at short wavelengths were reported by Vellekoop and Smit,[12–15] while Takahashi et al.[16,17] reported the first devices operating in the long-wavelength window. Dragone extended the concept from 1 × N DeMUX to N × N devices, the so-called wavelength routers,[18,19] which play an important role in multiwavelength network applications. AWGs are known by several different names: optical phased arrays (PAs), phased-array waveguide gratings (PAWGs), or waveguide-grating routers (WGRs). The acronym AWG, introduced by Takahashi,[16] is the most frequently used name today.

AWGs are considered an attractive DWDM solution because they represent a compact means of offering higher-channel-count technology, have good performance characteristics, and can be more cost-effective per channel than other methods. Compared to other technologies, they may also offer a quicker design cycle time, a uniform product, and the potential for easier scalability due to large commercial volumes.[20]

A further advantage of AWGs is that they can be included in a more complex management system, such as optical add-drop multiplexers (OADMs),[21] or with variable optical amplifiers (VOAs).[22,23] With the recent development and growth of the fiber-to-the-x (FTTx) market, the AWGs have also been used for CWDM applications where a much lower number of transmitting optical signals is required.[24] In next-generation access networks (NGANs), AWGs have been found to be highly suitable as optical coders/encoders that can generate and process optical codes directly in the optical domain.[25] A comprehensive overview of AWGs and their applications to date can be found in Ref. 26.

3.1 Principle

An AWG MUX/DeMUX is a planar device with both imaging and dispersive properties. It consists of I/O waveguides, the number of which usually equals the number of transmitting channels; an array of waveguides (also called phased array, PA); and two star couplers [also called a free-propagation region (FPR)], as shown in Fig. 5. The waveguides in the PA are spaced at regular intervals, with a constant path-length increment ΔL from one to the next, and join the star couplers at each end.

AWGs can function both as wavelength division MUX and DeMUX. An example of the operating principle of an AWG configured for spectral demultiplexing can be seen in Fig. 5. In this configuration, the input star coupler is an expanding free-propagation region where the light beam becomes divergent, while the output star coupler functions as a focusing FPR where each spectrally separated light beam is focused at one well-defined point on the focal line. Operation of the AWG DeMUX can be explained as follows: one of the input waveguides (usually the waveguide positioned at the center of the object plane of the input star coupler) carries an optical signal consisting of multiple wavelengths, $\lambda_1 - \lambda_n$ into the coupler. Once in the coupler, the light beam is no longer confined laterally and thus expands. The array waveguides capture this diverging light, which then propagates toward the input aperture of the output star coupler. The length of array waveguides is selected so that the optical path length difference between adjacent waveguides, ΔL, equals an integer multiple of the central wavelength, λ_c, of the DeMUX. For this wavelength, the fields in the individual arrayed waveguides will arrive at the input aperture of the output coupler with equal phases, and the field distribution at the output aperture of the input coupler will be reproduced at the input aperture of the output coupler. In the output star coupler, the light beam interferes constructively and converges at one single focal point on the focal line. In this way, for the central wavelength λ_c, the input field at

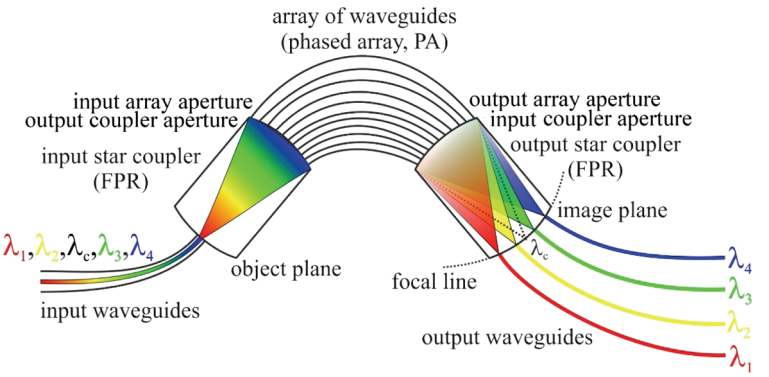

Figure 5 Principle of an AWG optical DeMUX.

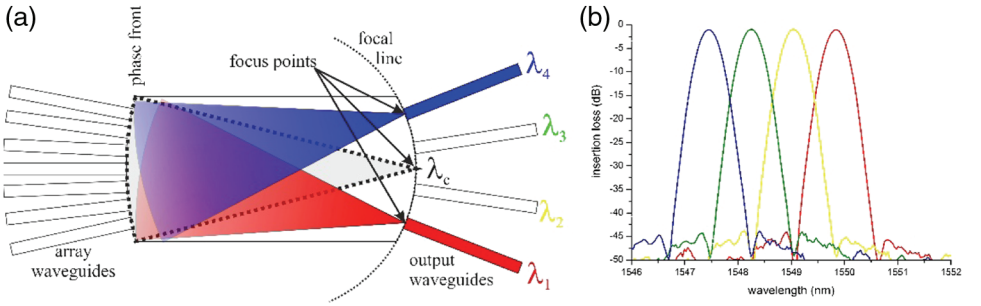

Figure 6 (a) Focusing the wavelengths on different positions of the focal line with four demultiplexed wavelengths. (b) The result is called an AWG spectral response.

the object plane of the input star coupler is transferred to the center of the image plane of the output star coupler.

If the wavelength is shifted to $\lambda_c \pm \Delta\lambda$ (i.e., λ_1, λ_2, ...), there will be a phase change in the individual PA waveguides that increases linearly from the lower to the upper channel. As a result, the phase front at the input aperture of the output star coupler will be slightly tilted, causing the beam to be focused on a different position of the focal line in the image plane (Fig. 6). By placing a waveguide in the correct position, the field for each wavelength can be coupled into the respective output waveguide (also called the transmitting channel).[27,28]

3.2 Different AWG types

Various AWGs are available on the market today and their optical characteristics depend largely on the optical properties of the waveguide materials used. AWGs can be fabricated on various material platforms such as silica-on-silicon (SoS) buried waveguides,[29–33] silicon-on-insulator (SOI) ridge waveguides,[34] SOI-nanowires,[35–37] buried InP/InGaAsP ridge waveguides,[38–41] polymer waveguides,[42–44] or Si_3N_4 waveguides.[45–47] In terms of material, they can all be divided into two main groups, the so-called low-index-contrast and high-index-contrast AWGs.

Low-index-contrast AWGs (SoS-based waveguide devices) were introduced to the market in 1994.[48] For the most part, they use SiO_2-buried rectangular waveguides, usually with a cross-section of $(6 \times 6)\ \mu m^2$ and a low refractive-index contrast between the core (waveguide) and the cladding, $\Delta n \sim 0.011$ [where the refractive index of the core $n_c \sim 1.456$ and the refractive index of the cladding $n_{cl} \sim 1.445$, as shown in Fig. 7(a)]. This parameter is also often expressed in percent as $\Delta n \sim 0.75\%$, from $(n_c - n_{cl})\cdot 100/n_c$. Low-index-contrast AWGs still hold a large share of the AWG market because of their many advantages. First, their modal field matches well with that of single-mode optical fibers, making it relatively easy to couple them to fibers [Fig. 7(c)]. Second, they combine low propagation loss (<0.05 dB/cm, because there is little absorption and scattering in the

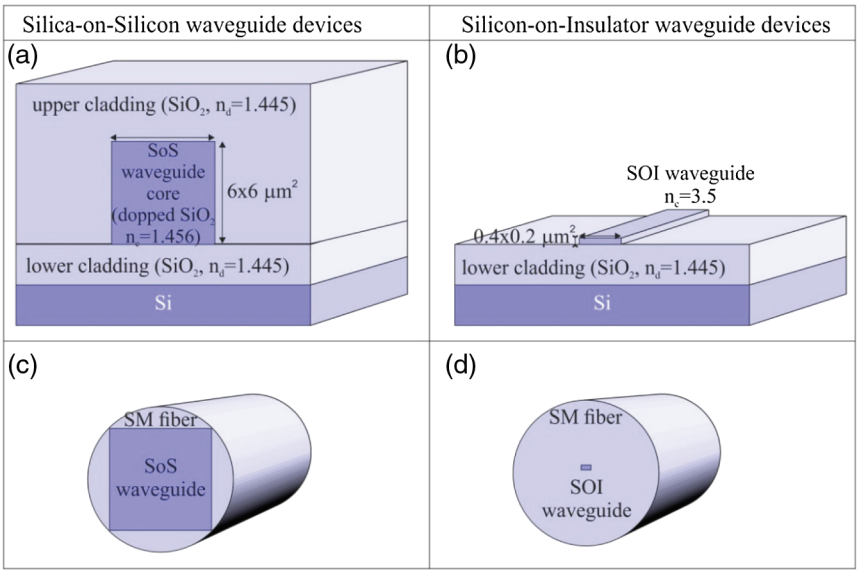

Figure 7 (a) and (b) Cross-sections of SoS and SOI waveguides with typical dimensions and refractive indices. (c) and (d) Comparison of the waveguide dimensions with the standard SM fibers.

waveguides) with a high fiber-coupling efficiency (low losses on the order of 0.1 dB).[48] However, the very low refractive-index contrast means the bending radius of the waveguides needs to be very large (on the order of several millimeters) and may not fall below a particular, critical value. As a result, silica-based AWGs usually have a very large size of several square centimeters that limits the integration density of SiO_2-based photonic integrated devices.

High-index-contrast AWGs, such as SOI-based waveguide devices, use a high refractive-index difference $\Delta n \sim 2.055$ for Si/SiO_2 (~2.5 for Si/air) between the refractive indices of the core (Si, $n_c \sim 3.5$) and the cladding (SiO_2, $n_{cl} \sim 1.445$, or air, $n_{cl} = 1.0$), as shown in Fig. 7(b) (in percent, $\Delta n \sim 58\%$). This is approximately 100 times higher than that of typical SoS waveguides. Due to the fact that a waveguide's size decreases proportionally to the increase in refractive index contrast, the waveguide size for this material composition shrinks into the nanometer scale [Fig. 7(b)]. Such high-index contrast makes it possible to guide light in waveguides with a far smaller bending radius (bending on the scale of several tens of microns), which leads to a significant reduction in the size of AWGs by more than two orders of magnitude when compared to AWGs based on silica materials.[49–51] Such compact devices can easily be implemented on-chip and have already found applications in WDM systems as add-drop filters, channel monitors, routers, cross-connects, and wavelength converters for complex optical metropolitan and local area networks (LAN). Typically, the spectral resolution of an

AWG can be raised by increasing the interference order of the grating or the number of arrayed waveguides. As a result, SOI-AWGs have been used not only for WDM but also for other emerging applications, such as optical sensors, particularly optical chemical and biosensors, silicon devices for DNA diagnostics, and optical spectrometers for infrared spectroscopy.[52–54]

The main problem arising from the reduced size of waveguides is the coupling of the optical signal from the fiber into such small input waveguides [Fig. 7(d)], which causes much higher coupling losses, on the order of 10 dB, than in silica AWGs. The second drawback of high-index-contrast waveguides is the sensitivity of the mode index to the dimensional fluctuation of the waveguide core, which leads to a rapid increase in random phase errors in the fabricated array grating arms. These technological imperfections affect the AWG's performance by causing a marked increase in the crosstalk (measured crosstalk is normally >15 dB[55]). In addition, in Si-nanowire waveguides, the scattering loss (per unit of length) is much larger than the loss for conventional low-index-contrast waveguides due to the light scattering on imperfections of the fabricated waveguide sidewalls.[56] In order to reduce the roughness of these sidewalls and thus minimize such high-dimensional fluctuations, the SOI-nanowire AWGs require very-high-resolution fabrication technology that still presents a considerable challenge today. An alternative to high-index-contrast and low-index-contrast AWGs is the Si_3N_4 material platform, which has a moderate index contrast lying between both main groups.[45,46,57,58]

Based on the applications, AWGs can be categorized according to the number of transmitting channels, channel spacing, and the spectral response.

Number of channels: As the number of transmitting channels (wavelengths) used to carry the information in WDM systems is generally a power of 2, the AWGs are designed to separate two different wavelengths (or 4, 8, 16, 32, 64, and so on). In addition, AWGs with 40 and 80 channels are also available.

Channel spacing: The wavelengths being used in transmitting channels are usually around the 1550-nm region, the wavelength region in which optical fiber performs best due to very low losses. Each wavelength is separated from the previous one by a multiple of 0.8 nm (also referred to as 100-GHz spacing, which is the frequency separation, Fig. 2). Thus, wavelengths can also be separated by 1.6 nm (i.e., 200 GHz) or any other channel spacing that represents a multiple of 100 GHz (0.8 nm). Systems with channel spacings of 100 GHz or higher are classified as WDM systems. However, as increasing capacity demands make it desirable to squeeze even more wavelengths into an even tighter space, systems are being designed with as little as half the regular spacing, i.e., 0.4 nm = 50 GHz, or even a quarter, i.e., 0.2 nm = 25 GHz. Systems with these narrow channel spacings are classified as DWDM systems. As the demand for higher capacity continues to grow, it will be necessary to keep raising the channel counts of AWGs as far as possible, thereby decreasing their channel spacing down to 12.5 GHz (=0.1 nm), 10 GHz (=0.08 nm), or less.

These AWGs with extremely narrow channel spacing will play a major role in the future of optical networks.

Spectral response: Based on spectral response, an AWG can be classified as a Gaussian type or a flat-top type. The most common is the Gaussian shape [Fig. 8(a)], which features very low insertion loss but is also limited by the influence of external factors due to its narrow 3-dB bandwidth (B@3 dB parameter, Section 3.5.1).[59] In contrast, the flat-top shape [Fig. 8(b)] suffers far higher insertion losses but features much better detection conditions (i.e., higher tolerance to laser wavelength deviations from the given channel center wavelength).[60–65] Somewhere between these two shapes lies a semiflat shape [Fig. 8(c)] that is also used in DWDM systems.[66]

Colorless AWG: A special member of the AWG family is the so-called "cyclic" or "colorless" AWG with 100- or 50-GHz channel spacing and 8 (or 16) output channels.[68–72] By applying a special design, such an AWG will repeat its orders and can work in any predefined channel band. In other words, the same colorless AWG can work on channels 1 to 8 or 9 to 16 or 17 to 24, and so on, as shown in Fig. 9, where each color represents the wavelengths focused to the

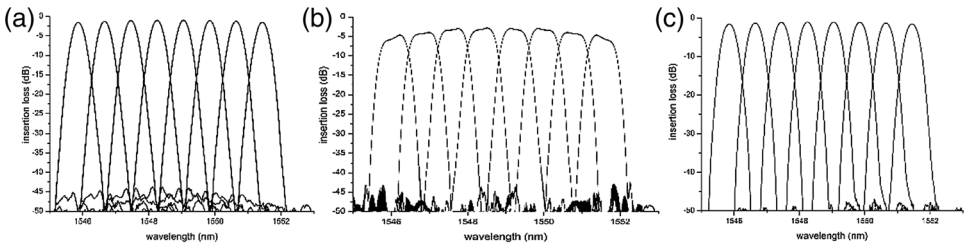

Figure 8 Different spectral responses of an 8-channel, 100-GHz AWG: (a) Gaussian shape, (b) flat-top shape, and (c) semiflat shape.[67]

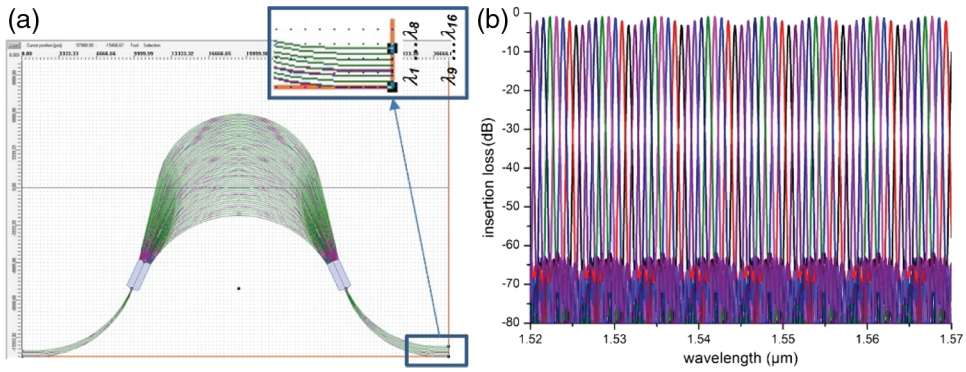

Figure 9 (a) 8-channel, 100-GHz colorless AWG: layout (b) with simulated transmission characteristics.[67]

same output waveguide. The principle and design of the 8-channel, 100-GHz colorless AWG are described in detail in Section 3.12.2.

3.3 Design

As already mentioned, an AWG can function both as a MUX and DeMUX. Most AWGs, however, are usually designed as a DeMUX because the spectral separation of the wavelengths is a much more challenging task.

The designs of AWG DeMUX discussed in this Spotlight are based on the model of Smit and van Dam, explained in detail in Refs. 27 and 73. To facilitate a better understanding of further work presented in this Spotlight, this model will be described briefly here.

3.3.1 Focusing

The length difference ΔL between adjacent waveguides in the PA is responsible for the focusing effect and can be described by

$$\Delta L = m \cdot \frac{\lambda_c}{n_{\text{eff}}} = \frac{m \cdot c_0}{n_{\text{eff}} \cdot f_c}, \tag{1}$$

where m is the order of the PA, $\lambda_c(f_c)$ is the central wavelength (frequency) in a vacuum, n_{eff} is the effective index of the waveguide mode, and c_o is the speed of light in vacuum. In this case, the array acts as a lens with image and object planes (Fig. 5) at a distance R_a from the array apertures (Fig. 10). Parameter ΔL is the first important parameter in the AWG design. Parameter R_a is the second AWG parameter, often called the focusing length of the star coupler, *Lf*.[74]

3.3.2 Dispersion

Another important parameter is dispersion, which determines the separation of the output waveguides on the center lines, *dx*, also known as the minimum waveguide

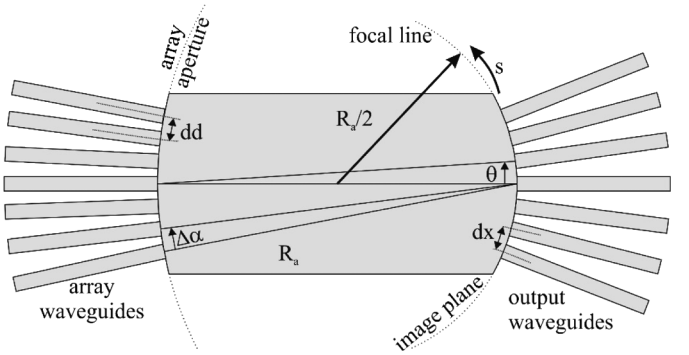

Figure 10 Geometry of the output star coupler.

separation between output waveguides[75] (Fig. 10). As can be seen in Fig. 10, the dispersion angle θ resulting from a phase difference ΔΦ between adjacent waveguides is given by

$$\theta = \arcsin\left(\frac{(\Delta\Phi - m\cdot 2\pi)/\beta_{\mathrm{FPR}}}{dd}\right) \sim \frac{\Delta\Phi - m\cdot 2\pi}{\beta_{\mathrm{FPR}}\cdot dd}, \tag{2}$$

where $\Delta\Phi = \beta\cdot\Delta L$, β and β_{FPR} are the propagation constants of the waveguide mode and the slab mode in the FPR, and *dd* is the lateral spacing (on the center lines) of the waveguides in the array aperture. It is also known as the minimum waveguide separation between PA waveguides.[75] *dd* is the fourth design parameter. From the dispersion angle, the dispersion *D* follows as

$$D = \frac{ds}{df} = R_a\cdot\frac{d\theta}{df} = \frac{1}{f_c}\cdot\frac{n_g}{n_{\mathrm{FPR}}}\cdot\frac{\Delta L}{\Delta\alpha}, \tag{3}$$

where *ds*/*df* is a lateral displacement of the focal spot along the image plane per unit frequency change, n_{FPR} is the slab mode index in the FPR, $\Delta\alpha = \frac{dd}{R_a}$ is the divergence angle between the array waveguides in the fan-in and fan-out sections, and n_g is the group index of the waveguide mode

$$n_g = n_{\mathrm{eff}} + f\cdot\frac{dn_{\mathrm{eff}}}{df}. \tag{4}$$

3.3.3 Free spectral range

An important property of the AWG is the free spectral range (FSR), also known as the DeMUX periodicity. This periodicity results from the fact that constructive interference at the image plane of the output coupler can occur for a number of wavelengths. In Fig. 11(a), each color represents the wavelengths focused to the same output waveguide [as in the case of the colorless AWG in Fig. 9(b)].

The fact that periodicity occurs is also clear from Eq. (2) where after each change of 2π in Δϕ, the field will be imaged at the same position. The period in

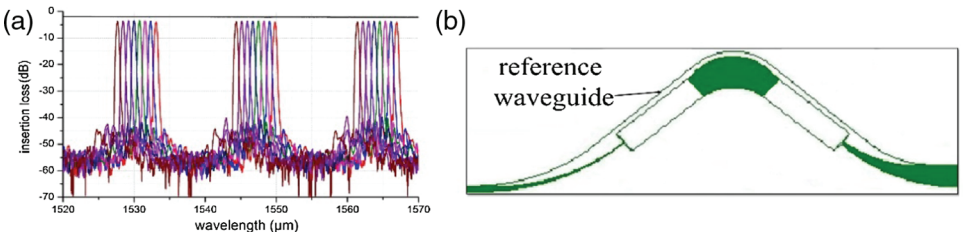

Figure 11 (a) Measured transmission characteristics of an 8-channel, 100-GHz AWG[67] and (b) AWG layout with reference waveguide.

the frequency domain is called the FSR, as presented in Fig. 12(b). The FSR is then given by

$$\Delta f_{\mathrm{FSR}} = \frac{c_0}{n_g \cdot \Delta L} = \frac{f_c}{m'}, \tag{5}$$

where $m' = \frac{n_g \cdot m}{n_{\mathrm{eff}}}$. As a result, the FSR should be designed large enough to prevent the different wavelengths from focusing into the same output waveguide.

3.3.4 Performance parameters

Depending on the application, the AWG must meet certain performance parameters. These parameters, some of which are also used as input parameters in AWG design, are described in detail in Section 3.5.1. Three of the most important parameters—channel crosstalk, insertion loss, and non-uniformity—will be explained here.

Figure 12(a) shows the field in the image plane for four different wavelengths. It is the sum-field of the far-fields of all individual array waveguides. As the far-field intensity of the individual waveguides reduces away from the center of the image plane, the focal sum-field will do the same. If the wavelength is changed, it will move through the image plane and follow the envelope described by the far-field of the individual array waveguides. Using the Gaussian-beam approximation, the intensity of the far-field is found from

$$I(\theta) = I_0 \cdot e^{-2\theta^2/\theta_0^2}, \tag{6}$$

where θ_0 is the width of the equivalent Gaussian far-field

$$\theta_0 = \frac{\lambda}{n} \cdot \frac{1}{w_e \cdot \sqrt{2\pi}}, \tag{7}$$

where w_e is the effective width of the modal field.

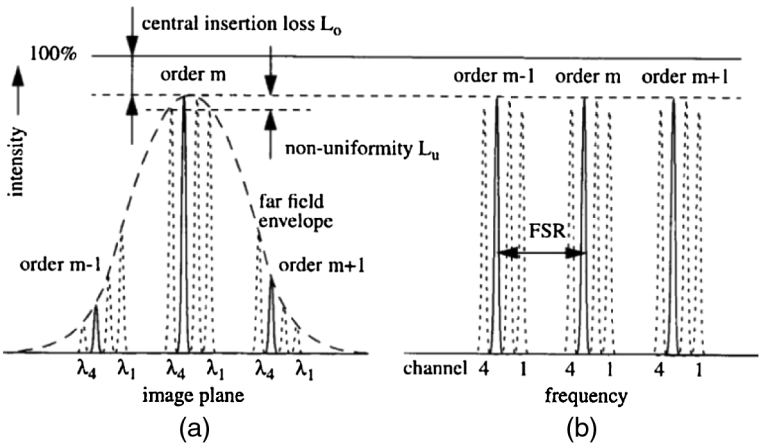

Figure 12 Central insertion loss L_0, non-uniformity L_u, and *FSR*. The 100% line denotes the peak intensity of the input field.[27,73]

3.3.5 Insertion loss

Fields propagating through an AWG are attenuated due to various loss mechanisms. The main sources for AWG insertion loss are

- the propagation loss in bent waveguides,
- the coupling loss between the fiber and the waveguide,
- the transition loss between the star couplers and arrayed waveguides, and
- the material and scattering losses.

Figure 12(a) shows the central insertion loss of the highest peak in the transmission characteristics L_o. It is the sum of all losses. As can be seen in Fig. 11(a), the straight black line is the loss (~2 dB) measured from the reference bent waveguide along the AWG structure shown in Fig. 11(b). This loss is caused mainly by the coupling losses between the fibers and the waveguides, the propagation loss in the bent waveguide, and the material and scattering losses. The difference between this line and L_o is additional loss coming from the AWG itself, i.e., the transition loss between the star couplers and arrayed/output waveguides.

3.3.6 Non-uniformity

Due to the fact that the wavelengths follow the envelope described by the far-field of the array waveguides, there will always be non-uniformity L_u in the intensity of focal sum-fields [Fig. 12(a)]. This parameter is defined as the intensity ratio (in dB) between the outer and the central channels. Using Eq. (6), L_u can be written as

$$L_u = -10 \cdot \log\left(e^{-2\theta_{\max}^2/\theta_0^2}\right) \approx 8.7 \cdot \frac{\theta_{\max}^2}{\theta_0^2}. \tag{8}$$

3.3.7 Channel crosstalk

Channel crosstalk describes the isolation of a particular transmitted channel from the other channels, and may also be called channel isolation. There are two types of channel crosstalk, i.e., adjacent and non-adjacent. By definition, adjacent (non-adjacent) channel crosstalk is an amount of unwanted power induced by a selected channel into adjacent (non-adjacent) transmitting channels, and vice versa (a full definition can be found in Section 3.5.1).

According to Smit,[27] there are many mechanisms that may cause crosstalk. Six sources are receiver crosstalk, aperture truncation, mode conversion, coupling in the array, phase transfer incoherence, and background radiation. The first four can be minimized by effective design, provided the fabrication process is sufficiently developed. The remaining crosstalk of a device with an optimized design stems almost exclusively from phase errors introduced by the fabrication process.

The most obvious source of crosstalk is caused by the coupling between the receiver sides of the star coupler (receiver crosstalk). Another cause of crosstalk is truncation of the propagation field due to the finite width of the output array

aperture. This truncation of the field produces a loss of energy and increases the output focal field side-lobe level. To obtain sufficiently low crosstalk, the array aperture angle of the AWG should be larger than twice the Gaussian width of the field. If this requirement is met, the truncation crosstalk should be lower than −35 dB. Crosstalk by mode conversion is caused by a "ghost" image of multimode junctions and can be minimized if the junction offset is optimized by avoiding first mode excitation. The crosstalk caused by coupling in the PA can be avoided by increasing the minimum separation between the array waveguides (parameter *dd*).

If, however, there are errors in the optical path length of the array grating arms, the phase acquired across them will no longer be linear, and the light will not focus to a clean point on the focal line of the image plane.[76] A wavelength intended to focus at a particular output waveguide will, therefore, couple incorrectly to neighboring output waveguides, too, thus causing higher adjacent channel crosstalk. These distortions are known as phase errors and are caused by variations in the effective length of the array grating arms due to fabrication errors or wafer non-uniformity.[77,78] For this reason, on a practical level, the reduction of crosstalk for a design-optimized AWG device is limited by imperfections in the fabrication process.

3.3.8 Design parameters

The AWG design begins with the calculation of its dimensions, which are essential to create the AWG layout. The dimensions are given by the geometrical parameters, as shown in Fig. 13, and can be calculated from the model of Smit and van Dam that was introduced at the beginning of this section. Four of these parameters determine the optical properties of an AWG:

- minimum waveguide separation between the PA waveguides (*dd*),
- minimum waveguide separation between the I/O waveguides (*dx*),
- length of the star coupler (*Lf*), and
- length difference between adjacent waveguides in the PA (ΔL).

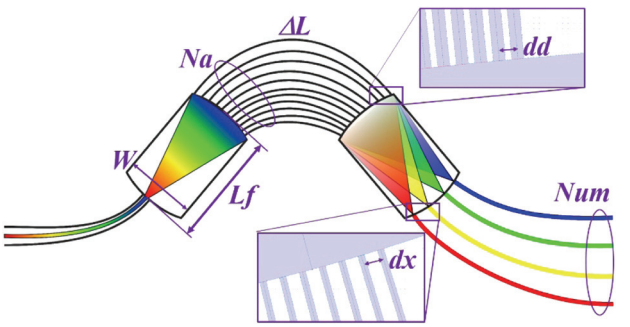

Figure 13 Geometrical parameters used in the AWG design.

In general, the *dd* parameter should be as small as possible to achieve a compact design for the AWG MUX/DeMUX. However, this parameter is dependent on the resolution of the fabrication technology.

In order to achieve sufficient isolation between output transmitting channels, the parameter *dx*, i.e., the minimum waveguide separation between output waveguides, should be sufficiently large and, as a general rule, at least twice the width of the waveguide.[74]

The impact of the length of the couplers *Lf* on the non-uniformity L_u can be seen clearly in Fig. 12(a). The longer the output coupler, the wider the far-field intensity in the image plane. Taking into account the constant parameter *dx* (separation between output waveguides) and keeping the number of output channels *Num* constant, it follows that the longer the coupler is, the smaller the non-uniformity will be.

The width of the coupler, *W*, is not a dominant parameter. However, it should be no smaller than the width of the far-field intensity in the output aperture of the input star coupler,[79] as shown in Fig. 14(b). This figure shows the simulated spectral response of a 32-channel, 100-GHz AWG using two different widths of couplers. As can be seen, a design that incorporates couplers too narrow in width [Fig. 14(a)] leads to a deterioration of the AWG spectral response, as shown in Fig. 14(c).

The number of array waveguides, *Na*, is usually calculated from the width of the far-field intensity in the output aperture of the input star coupler *W* [Fig. 14(b)],

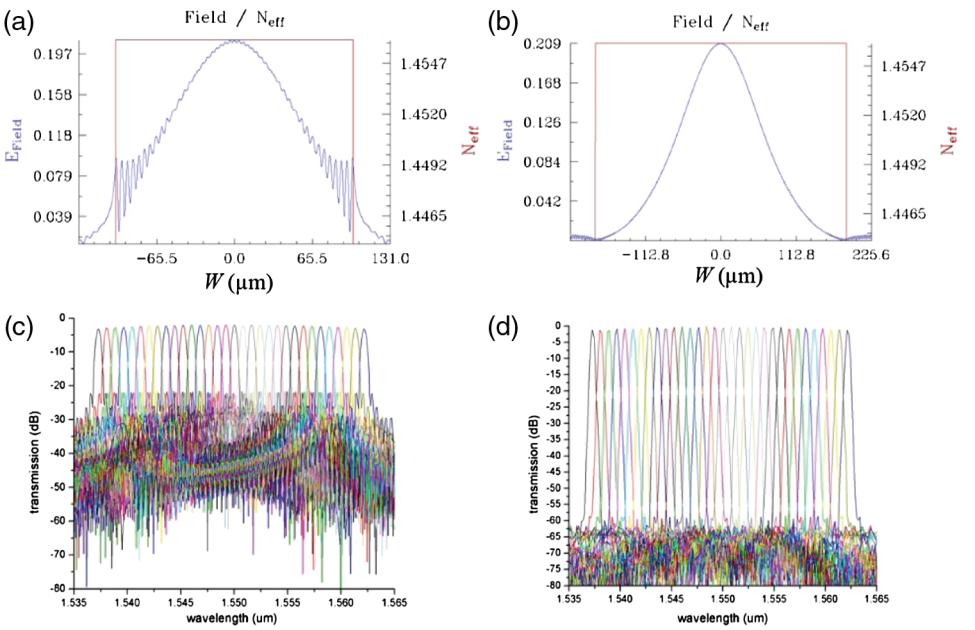

Figure 14 32-channel, 100-GHz AWG design: (a) and (b) far-field intensity in the output aperture of the input star coupler; (c) and (d) AWG spectral responses.

divided by the minimum waveguide separation between PA waveguides ($Na \sim W/dd$). In this way, all of the light in the input star coupler is collected by the input array aperture. As a general rule, this number should be greater than four times the number of output transmitting channels, *Num*.[74]

3.3.9 Input parameters for AWG design

In order to calculate AWG geometrical parameters (i.e., *dd*, *dx*, *Lf*, and ΔL), a set of input parameters is required:

- **Technological parameters:** Each AWG is designed for a particular material platform, such as SoS, SOI, Si_3N_4, and so on. The materials used are described by the refractive indices of the core (waveguide) n_c and the cladding n_{cl}. By taking into account the size of the waveguide structure as well [waveguide cross-section presented in Fig. 7(a)], it is possible to calculate the effective refractive index n_{eff} and group refractive index n_g.
- **AWG-type parameters:** These are determined based on the requirements of the WDM/DWDM network and the customers. Each AWG is designed for a particular central wavelength λ_c, having a certain number of transmitting channels (=output waveguides, parameter *Num*) and channel spacing *df*. Usually the channel spacing is selected according to the ITU-grid standard, e.g., 50 GHz, 100 GHz, and so on.
- **Transmission parameters:** Each AWG is designed for a particular application and must, therefore, meet certain target specifications. These specifications describe the performance of an AWG and are given in the form of performance (transmission) parameters. They are usually calculated from the AWG spectral response (also called transmission characteristics).

Before describing the AWG design, it is necessary to point out that all AWGs designed and presented here are low-index-contrast AWGs with a typical refractive index difference of 0.75%, where the refractive index of the cladding n_{cl} = 1.445, and the refractive index of the core n_c = 1.456. For such low-index-contrast AWGs, the standard cross-section of a waveguide structure is typically (6 × 6) μm^2 to ensure single-mode propagation only [Fig. 7(a)]. All optical DeMUX were designed for the AWG central wavelength λ_c = 1550 nm.

As there is a strong correlation between the dimensions of the AWG structure and its performance, the AWG geometrical parameters have to be calculated with a high degree of precision. For these calculations, the model of Smit and van Dam (Section 3.3) was used. Once all of the geometrical parameters have been calculated, they can be used to create the AWG layout. Several commercially available photonics software tools, such as Apollo Photonics, RSoft, Optiwave or Photon, can be used to create and to simulate the AWG layout [Fig. 15(b) shows the AWG layout of an 8-channel, 100-GHz AWG created by the Apollo Photonics tool]. The output of the simulation is an AWG spectral response for both the transverse electric (TE) and the transverse magnetic (TM) polarization states

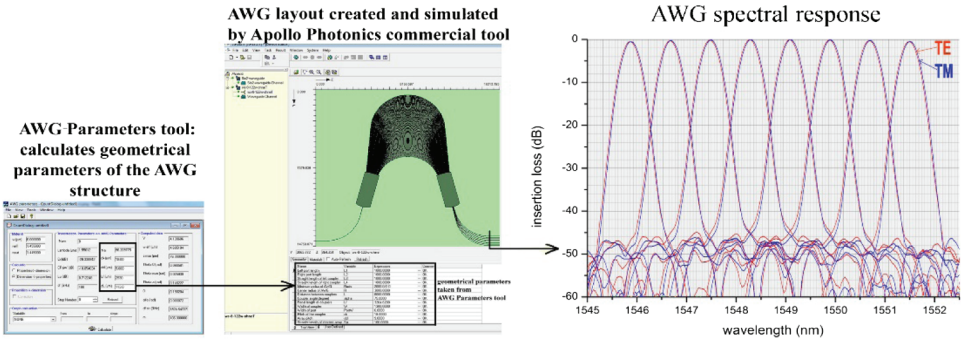

Figure 15 Design and simulation of an 8-channel, 100-GHz AWG.

[transmission characteristics, Fig. 15(c)]. At this point, it is important to note that various different terms are used in the literature to describe transmission characteristics. Figure 15(c) shows "insertion loss" as a function of wavelength, but the words "transmittance," "power," "output power," "loss," or "transmission" are also very common.

3.3.10 AWG-Parameters tool

As the commercial photonics tools do not support (or only partially support) the calculation of the AWG geometrical parameters, the first calculations were done manually and were, therefore, very time-consuming. This led to the development of a new software aid called the "AWG-Parameters" tool[80,81] [Fig. 15(a)]. This tool significantly reduces the time needed for AWG design and also facilitates an understanding of the relationship between input design and geometrical parameters.

For the purpose of explaining the functionality of the AWG-Parameters tool, a standard Gaussian 8-channel, 100-GHz AWG design was selected as an example. The input parameters for the calculation of its geometrical parameters are as follows:

Technological parameters: Used to design the waveguide structure ("Material" window in Fig. 16):

- Waveguide structure: waveguide width w = 6 μm [from Fig. 7(a)].
- Refractive indices: n_{eff} (effective index) = 1.455003, n_{out} (cladding n_{cl}) = 1.445.

AWG-type parameters ("Transmission Parameters → AWG-Parameters" window in Fig. 16):

- Number of output transmitting channels: *Num* = 8.
- AWG central wavelength (λ_c): *Lambda* (μm) = 1.55012.
- Channel spacing: *df* (GHz) = 100.

Transmission parameters ("Transmission Parameters → AWG-Parameters" window in Fig. 16):

- Adjacent channel crosstalk between output waveguides: Cr (dB) = −30.
- Adjacent channel crosstalk between arrayed waveguides: $CRaW$ (dB) = −10.
- Uniformity over all output channels (also called non-uniformity): L_u (dB) = 0.7.

When the "Calculate" button is pressed, the tool calculates all of the necessary geometrical parameters in the "Transmission Parameters → AWG-Parameters" window (Fig. 16):

- Number of arrayed waveguides: Na = 100.951257.
- Minimum waveguide separation between I/O waveguides: dx (μm) = 19.328944.
- Minimum waveguide separation between PA waveguides: dd (μm) = 8.97488.
- Coupler length: Lf (μm) = 3007.77618.
- PA waveguide length difference (ΔL): dL (μm) = 111.621329.

The tool also offers the function "Calculate" ("Calculate" window in Fig. 16), a very important function that allows calculation of the geometrical parameters from the transmission parameters ("Properties → dimension") and vice versa ("Dimension → properties"). This function can be used to simplify the alignment of calculated geometrical parameters to the technological requirements. For example, accuracy of the calculated minimum waveguide separation in the PA,

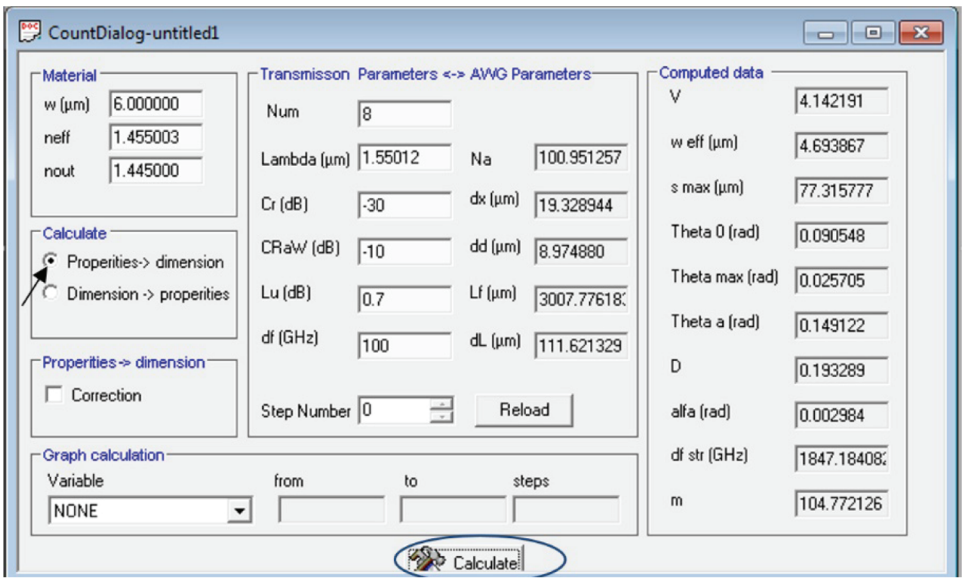

Figure 16 User interface of the AWG-Parameters tool.

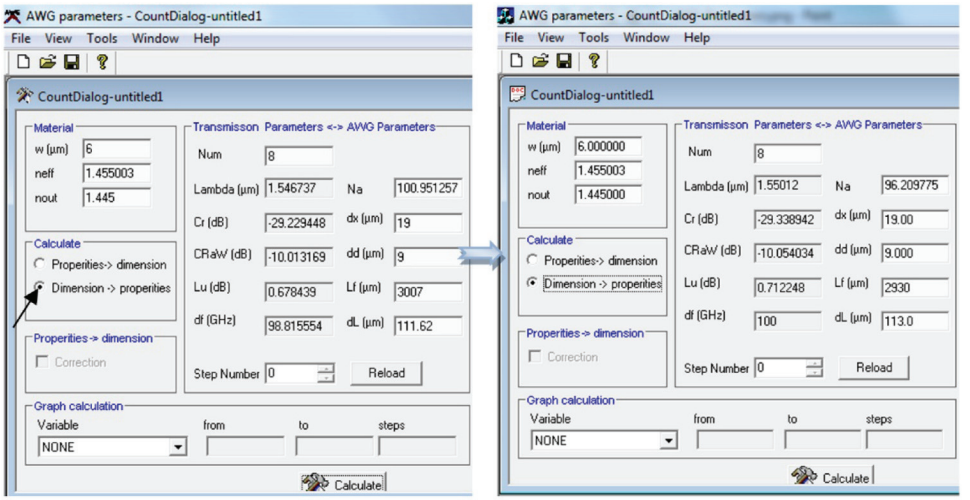

Figure 17 Calculated geometrical parameters of the (a) 8-channel 100-GHz AWG and (b) after several iterations, using the AWG-Parameters tool.

dd (µm) = 8.974880 (Fig. 16) is more difficult to achieve technologically than *dd* (µm) = 9 calculated using the function "Dimension → properties" [Fig. 17(a)]. Similarly, accuracy of the parameter *dx* (µm) = 19 [Fig. 17(a)] is much easier to achieve technologically than *dx* (µm) = 19.32894 in Fig. 16. Figure 17(b) shows the final calculated geometrical parameters of the designed 8-channel, 100-GHz AWG.

3.3.11 Design optimization

It is important to point out that any geometrical parameter adjustment has an influence on the transmission parameters as presented in the left column of Fig. 17(a) (parameters *Lambda*, *Cr*, *CRaW*, L_u, *df* have changed). Therefore, an immediate response to any change in AWG design (i.e., change of parameters *dx*, *dd*, *Lf*, *dL*) can be observed in its performance. As such, the "Dimension → properties" function can also be used to optimize existing AWG designs.

Additionally, the tool also enables the calculation of all passive parameters (shown in Fig. 18 as a fields with a gray background, in this case *Lambda*, *Cr*, *CRaW*, L_u, and *df*), by simply scanning just one of the active parameters (shown in Fig. 18 with a white background, i.e., *Num*, *Na*, *dx*, *dd*, *Lf*, and *dL*) and keeping the rest of these active parameters constant. As can be seen in the "Graph calculation" window, the *dL* parameter was scanned between 105 and 115 µm with 1000 steps. The parameters *Num*, *Na*, *dx*, *dd*, and *Lf* were kept constant, and parameters *Lambda*, *Cr*, *CRaW*, L_u, and *df* were calculated for each *dL*. The advantage of this scanning function is the ability to display the behavior of various parameters (each having its own *y* axis) together in one graph ("GRAPHview1" window in Fig. 18).

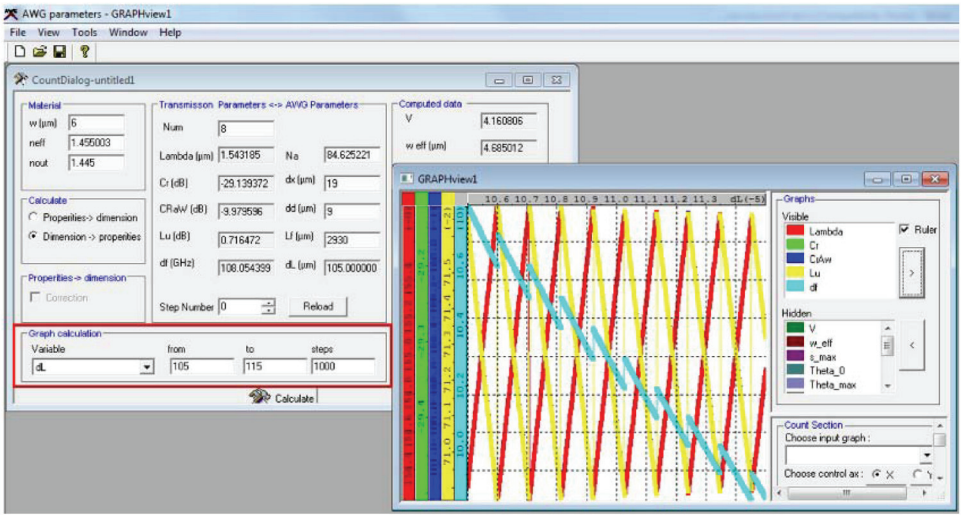

Figure 18 Scan function used in the AWG-Parameters tool.

3.4 Simulation of AWG layout

The calculated geometrical parameters of the 8-channel, 100-GHz AWG [i.e., *dx*, *dd*, *Lf*, and *dL* taken from Fig. 17(b)] were used as input for the commercial photonic tools to create the AWG layout and to carry out the beam propagation method (BPM) simulations [Fig. 19(a) shows this AWG layout using the Optiwave tool; it is the same AWG layout as in Fig. 15, created by the Apollo Photonics tool]. The output of the simulation, i.e., the transmission characteristics, is shown in Fig. 19(b). These characteristics create the basis for the calculation of AWG transmission parameters [Fig. 19(c)].

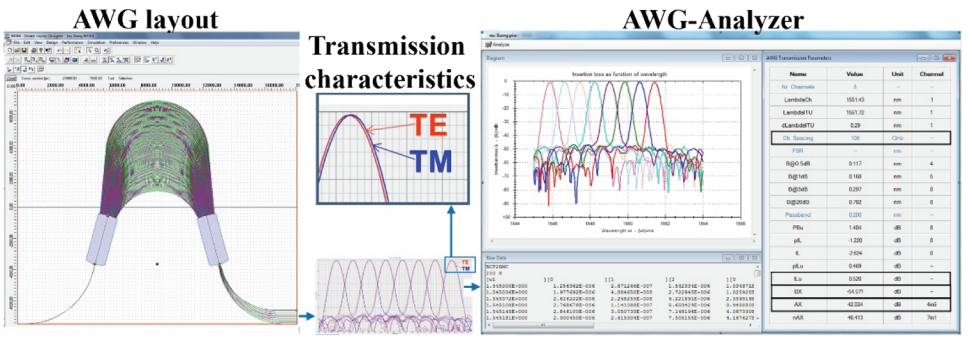

Figure 19 Simulated transmission characteristics of the 8-channel, 100-GHz AWG.

3.5 Evaluation of simulated AWG transmission characteristics

The performance of the designed AWG is defined by a set of transmission parameters that are extracted by analyzing AWG transmission characteristics. This is a complicated task because although the measurement method deployed by most AWG vendors is the Mueller matrix method,[82,83] the way that vendors specify the performance of a device from the measured curves differs widely. In addition, it is important to note that the output from all commercially available AWG design tools consists of simulated transmission characteristics only, and none of these tools supports (or supports only partially) the software-aided evaluation of AWG transmission parameter calculation.[74,75,84] The only possibility is to determine the AWG transmission parameters manually, directly out of the transmission characteristics graph. Major disadvantages of manual evaluation are that it is very cumbersome and time-intensive, and can also be imprecise due to reading errors especially for high-channel-count, narrow-channel-spacing or colorless AWGs. Manual evaluation can also cause the design, simulation, and fabrication of AWGs to be an extremely complicated matter because modifications of layout or the fabricated device always require a detailed evaluation of the current simulated or measured data. In addition, there is no uniform standard that applies to the evaluation of AWGs.[85] This means that the definitions of AWG transmission parameters are not yet standardized, resulting in the fact that no one is able to precisely determine the performance of an AWG, with the exception of those people involved in the design and/or fabrication of the AWG in question. Therefore, a sustainable evaluation should always provide clear definitions of how the AWG transmission parameters were determined. In summary, there are two major evaluation difficulties:

1. Definitions of the AWG transmission parameters are not standardized.
2. Manual evaluation is very cumbersome and time-consuming, and can be imprecise due to reading errors.

3.5.1 Definitions of AWG transmission parameters

To solve the first problem, extensive research on the definitions of AWG transmission parameters was carried out in the literature and also from various foundries that fabricated, measured, and evaluated designed AWGs.[67] Based on this knowledge, 19 transmission parameters, as presented in Table 1, were defined.

Number of output channels (*Nr. Channels*): Any AWG is designed to MUX/DeMUX a particular number of output channels available for data transmission. This is also an input parameter for AWG design (in Fig. 16 parameter *Num*).

Channel center wavelength (*LambdaCh*): The channel center wavelength is a real simulated or measured center wavelength of each optical signal [Fig. 20(a)].

ITU channel center wavelength (*LambdaITU*): ITU channel center frequencies (or ITU channel center wavelengths) allowed for optical data transmission [Figs. 2 and 20(a)].

Table 1 AWG transmission parameters calculated from the simulated/measured AWG transmission characteristics.[67]

Nr. Channels	Number of output channels
LambdaCh	Channel center wavelength
LambdaITU	The nearest ITU wavelength to the channel center wavelength
dLambdaITU	Channel center wavelength shift to the nearest ITU wavelength
Ch. Spacing	Wavelength/frequency spacing between two neighboring channels
FSR	Free spectral range
B@0.5 dB, *B@1 dB*, *B@3 dB*, *B@20 dB*	Width of the transmitted optical signal at a −0.5 dB, −1 dB, −3 dB and −20 dB drop from the transmission peak
Passband	Defined as a symmetrical wavelength range around each channel center wavelength (channel band)
Pbu	Passband uniformity (ripple)
pIL	Peak insertion loss measured from channel transmission peak to the 0 dB reference line
IL	Insertion loss of a channel measured within the passband to the 0 dB reference line
pILu	Peak insertion loss uniformity: the difference between maximum and minimum *pIL* over all the output channels
ILu	Insertion loss uniformity calculated within the passband of each channel over all the output channels
AX	Adjacent channel crosstalk
nAX	Non-adjacent channel crosstalk
BX	Background crosstalk

Channel center wavelength shift to the nearest ITU wavelength (*dLambdaITU*): The AWG should be designed to match ITU channel center wavelengths exactly. *dLambdaITU* defines the deviation of the real simulated/measured channel center wavelength from the nearest recommended ITU channel wavelength [Fig. 20(a)].

Channel spacing (*Ch. Spacing*: *df*/*dLambda*) is a separation in the frequency, *df*, or in the wavelength, *dLambda* between channel center wavelengths/frequencies of two adjacent channels [Fig. 20(b)].

FSR (*FSR*) is a period of the spectrum in the frequency domain [Fig. 12(b)]. *FSR* can be defined as the distance in frequency or wavelength between the center wavelengths of two adjacent orders of one channel [Fig. 20(c)].

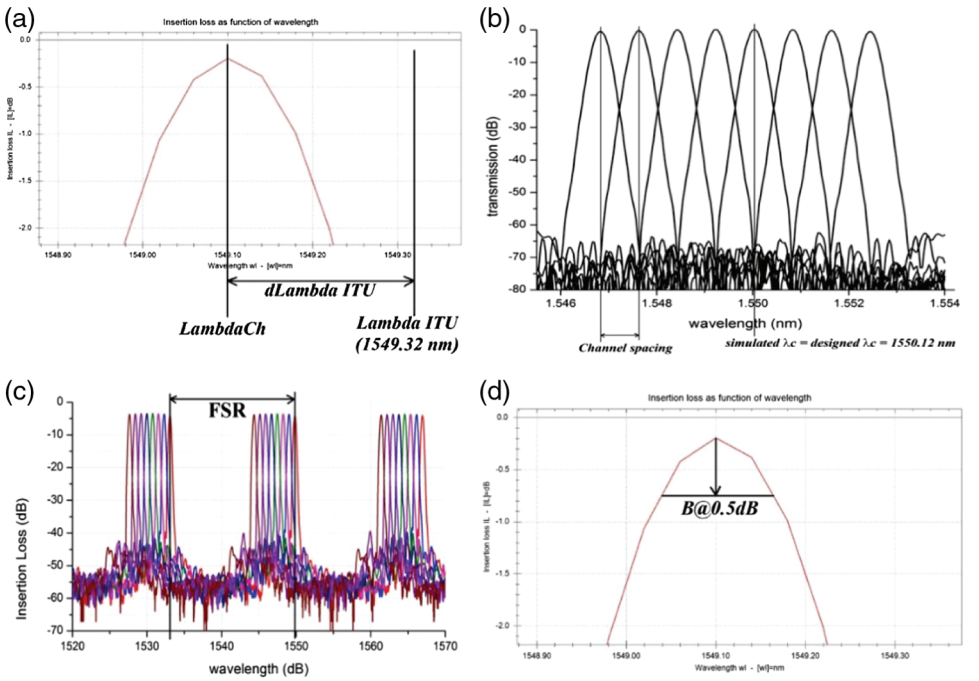

Figure 20 Graphical representation of the definitions of AWG transmission parameters without passband.

Bandwidth at −0.5 dB, −1 dB, −3 dB, and −20 dB (*B@0.5 dB*, *B@1 dB*, *B@3 dB*, and *B@20 dB*): This parameter defines the width of a transmitted optical signal at a −0.5 dB, −1 dB, −3 dB, and −20 dB drop from transmission peak [Fig. 20(d)].

Channel band (*Passband*): ITU band is defined as a symmetrical wavelength range around ITU frequencies usually having a width representing 25% of the channel spacing. Most of the AWG performance parameters are calculated within this band. Since there is often a channel center wavelength shift to the ITU wavelengths (*dLambdaITU*), we defined the channel band (passband), which is a symmetrical wavelength range around the channel center wavelengths (*LambdaCh*) also having a width of 25% of the channel spacing [Fig. 21(a)]. Most of the following transmission parameters are calculated within this passband. For all of these parameters, the worst case for each channel within the passband has been taken [e.g., Fig. 21(c), IL_{max}] and the final value then defined as the worst value over all output channels taking into account both polarization states [Fig. 21(d)].

Passband uniformity (ripple) (*Pbu*): *Passband* uniformity is the loss variation within the passband defined as the difference in dB between maximum and minimum transmissions [Fig. 21(b)].

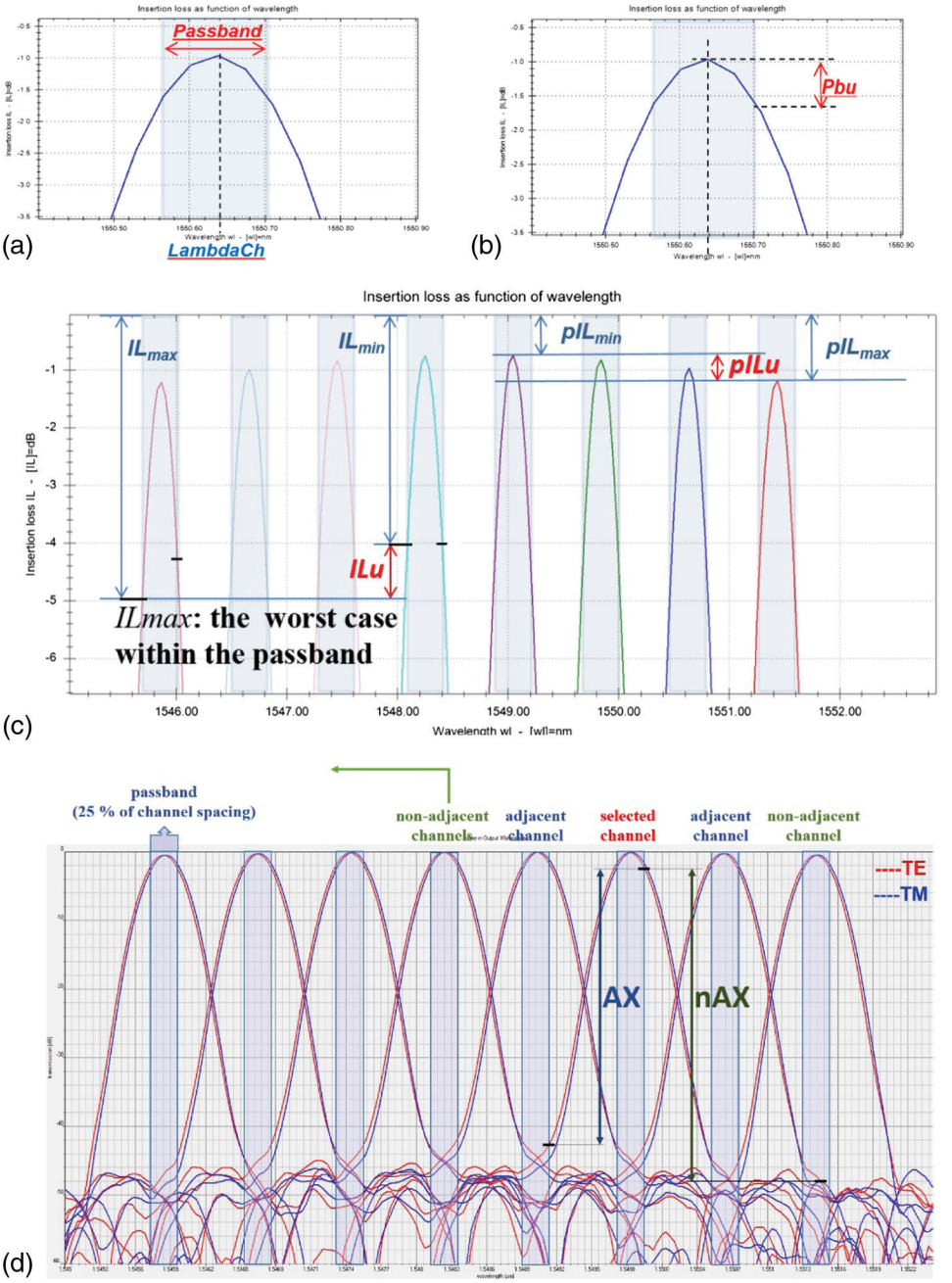

Figure 21 Graphical representation of the definitions of *Pbu*, *IL*, *ILu*, *AX*, and *nAX* transmission parameters.

Insertion loss: The loss of optical power occurs when light is coupled from the fiber into the input waveguide, from the output waveguide into the fiber, from the input coupler into the arrayed waveguides, and from the output coupler into the output waveguides, or when light propagates through the structure. It may also be caused by material absorption and scattering. The design of the AWG should be such that losses are minimized as far as possible. There are two different insertion loss parameters:

Peak insertion loss (*pIL*): The peak insertion loss of a channel is defined as the loss in power measured from the smallest transmission peak (pIL_{max}) in the transmission characteristics to the 0-dB reference line [Fig. 21(c)]. As can be seen, this parameter does not depend on passband.

Insertion loss (*IL*): Of greater importance is the insertion loss of a channel measured within the passband from the 0-dB reference line, *IL* [whereby the worst case is considered (IL_{max}), as can be seen in Fig. 21(c)]. This value is always worse than the parameter *pIL*.

Insertion loss uniformity: Insertion loss uniformity is the difference in the insertion losses between optical output signals (often called non-uniformity) and is always present. It follows the far-field intensity in the output coupler as shown in Fig. 12(a). It should be kept as low as possible, as it also increases the insertion loss parameter. There are two different parameters for insertion loss uniformity:

Peak insertion loss uniformity (*pILu*): Peak insertion loss uniformity is defined as the difference between the maximum and minimum peak insertion loss over all output channels [$pILu = abs(pIL_{max} - pIL_{min})$, Fig. 21(c)]. This parameter correlates with the theoretical non-uniformity L_u, as presented in Fig. 12(a), and does not depend on the passband.

Insertion loss uniformity (*ILu*): Insertion loss uniformity is defined as the difference between the worst case of insertion loss within the passband of each channel and then the worst value over all the channels [$ILu = abs(IL_{max} - IL_{min})$, Fig. 21(c)].

Adjacent channel crosstalk (*AX*): Adjacent channel crosstalk can be described as the unwanted power induced by a selected channel in the adjacent channel, and vice versa. It is defined as the worst case difference between the lowest transmission in the passband of the selected channel and the highest transmission of the selected channel in the passband of the adjacent channel. It indicates the worst value over all the channels [Fig. 21(d)]. A higher parameter value means better channel isolation, i.e., lower channel crosstalk. In the literature, another definition can also be found;[85] however, in principle, this definition leads to the same calculation of the *AX* parameter.

Non-adjacent channel crosstalk (*nAX*): The non-adjacent channel crosstalk can be described as the highest unwanted power induced by a selected channel in one of the non-adjacent channels. It is defined as the worst-case difference

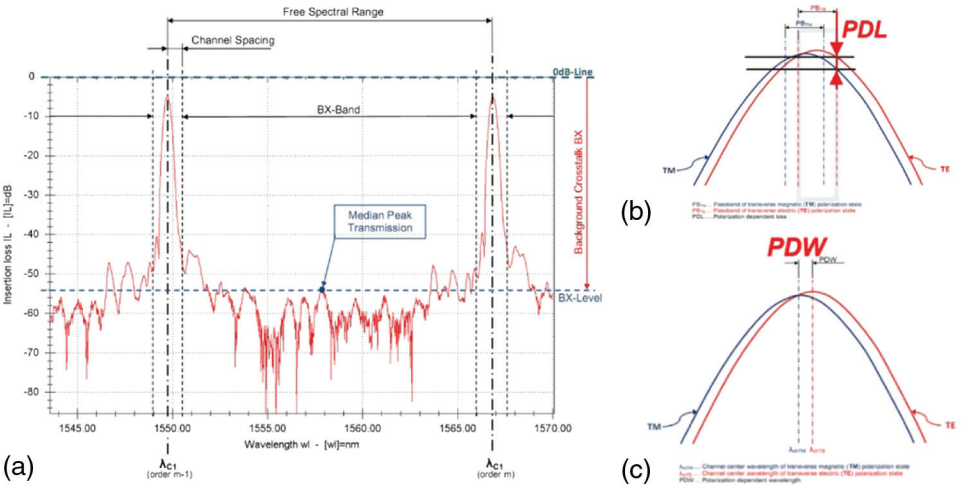

Figure 22 Graphical representation of the definitions of (a) *BX*, (b) *PDL*, and (c) *PDW* transmission parameters.

between the lowest transmission in the passband of the selected channel and the highest transmission of the selected channel in the passband of any non-adjacent channel. It represents the worst value over all the channels [see Fig. 21(d)]. The higher the value of this parameter, the better the channel isolation (i.e., smaller non-adjacent channel crosstalk).

Background crosstalk (*BX*): The background crosstalk is defined as the median peak transmission in the BX-band of the channel. The BX-band includes all wavelengths except in the region of the channel center wavelength ± channel spacing. It indicates the worst value over all channels [Fig. 22(a)]. The higher the parameter value is, the better the channel isolation.

Polarization-dependent loss (*PDL*): *PDL* is defined as the worst variation in insertion loss within the passband of a channel between both polarization states over all of the output channels as shown in Fig. 22(b).

Polarization-dependent wavelength (*PDW*): The *PDW* shift is defined as a deviation in the channel center wavelengths between both polarization states [Fig. 22(c)]. This parameter does not depend on the passband.

3.5.2 AWG-analyzer tool

In order to resolve the problem of manual evaluation, a new software aid called the "AWG-Analyzer" tool was developed.[86,87] Figure 23 shows the tool's user interface, which is divided into three windows:

- Raw data (textual representation): The content of original input file (consisting of simulated or measured data) is displayed in the "raw data" window.

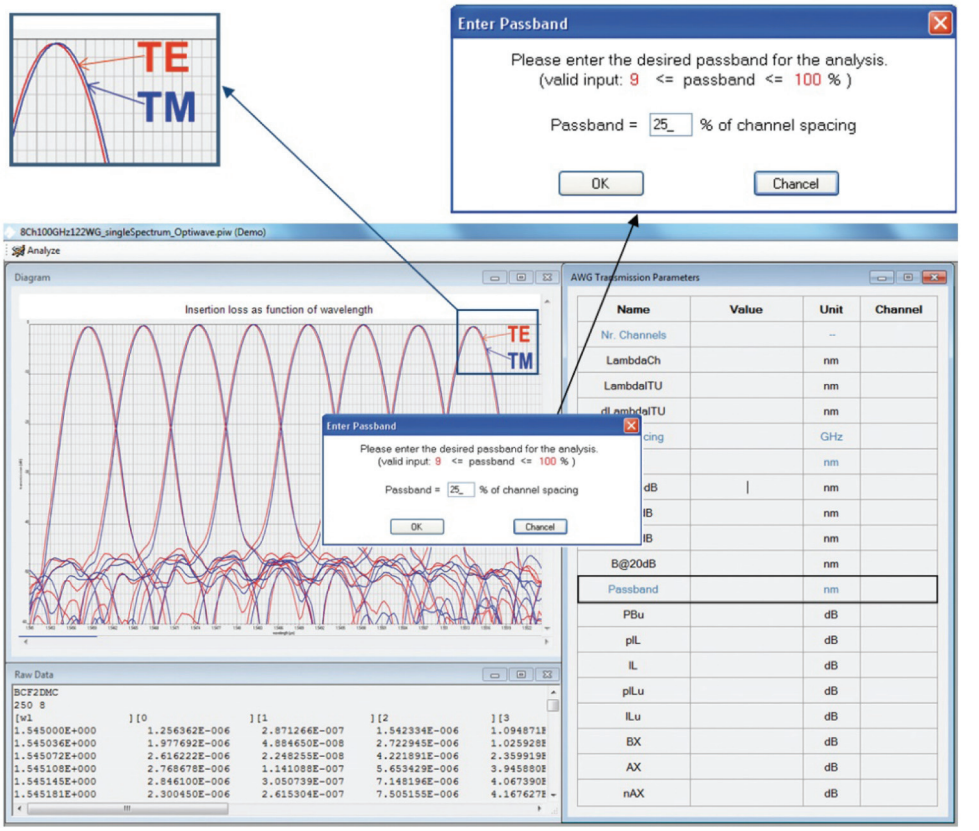

Figure 23 User interface of the AWG-Analyzer tool.

- Diagram: A graphical representation of raw data is displayed in the "diagram" window.
- Transmission parameters: This view shows a table containing all the transmission parameters defined in the Section 3.5.1, with the exception of *PDL* and *PDW*. This parameter window provides two different views of the evaluated parameters. Figure 24 shows both the "AWG transmission parameters" view (a) and "All transmission parameters" view (b), including switching context menu and mouse hover options for the AWG transmission parameter, *LambdaCh*.

3.5.2.1 "AWG transmission parameters" view

This view shows a table containing all of the evaluated transmission parameters, their units, and their associated channels. Figure 24(a) shows the transmission parameters view from the evaluated transmission characteristics of the designed and simulated 8-channel, 100-GHz AWG.

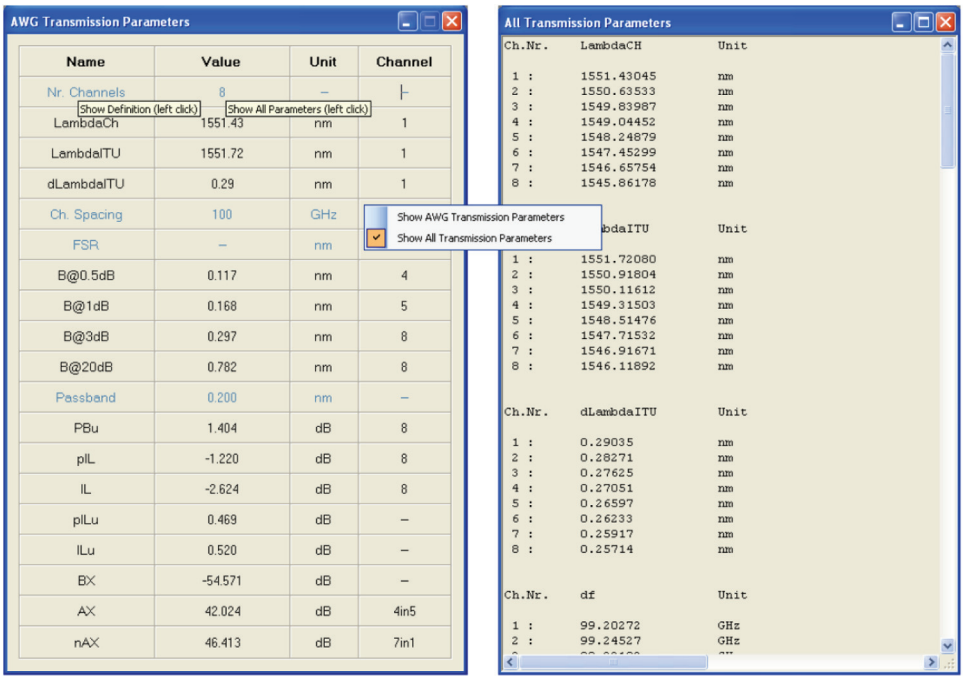

(a) (b)

Figure 24 (a) "AWG transmission parameters" view and (b) "All transmission parameters" view available in the parameter window.

3.5.2.2 "All transmission parameters" view

This view displays all transmission parameters evaluated by the software tool over all channels' blocks containing channel numbers, values, and units of the parameters.

The tool offers some other supporting functions:

- **User-defined passband value:** As already mentioned, the parameter *passband* usually equals 25% of the channel spacing. However, to be able to calculate the transmission parameters for any passband value, this parameter is implemented as a variable input quantity (Fig. 23).
- **Help for each calculated AWG transmission parameter:** The tool can display a textual and graphical definition of each parameter from Table 1 at any time (Fig. 25). All transmission parameter calculations implemented in the evaluation algorithm of the AWG-Analyzer tool are performed according to these definitions. These textual and graphical definitions are implemented in the software's help system.
- **Recognition of various spectra:** The tool recognizes whether the file contains measured or simulated data of single spectrum transmission characteristics (Fig. 25), multiple spectrum transmission characteristics (consisting

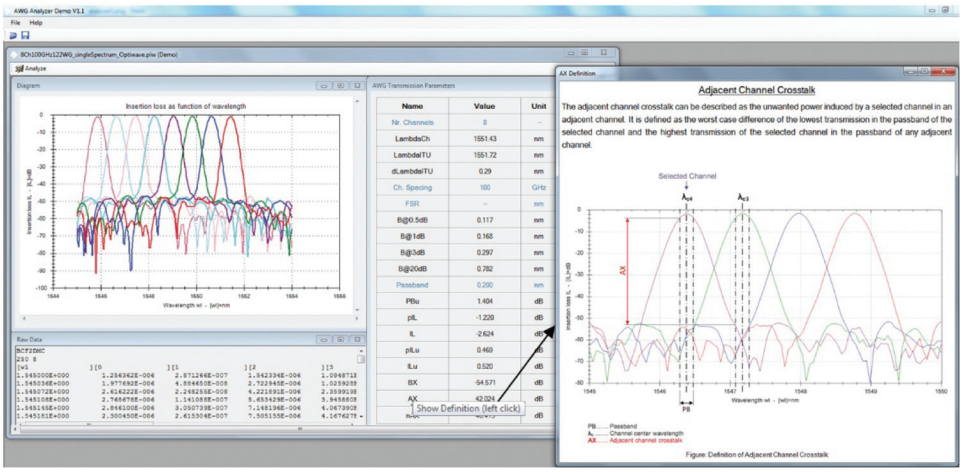

Figure 25 Textual and graphical definitions implemented in the software's help system are available at any time.

of multiple orders of the PA response with *FSR*), as shown in Fig. 26, or colorless spectrum characteristics [Fig. 9(b)].

- **AWG datasheet:** To summarize the evaluation results, the AWG-Analyzer tool generates an evaluation sheet (datasheet) containing the evaluated transmission parameters and a diagram of the transmission characteristics.

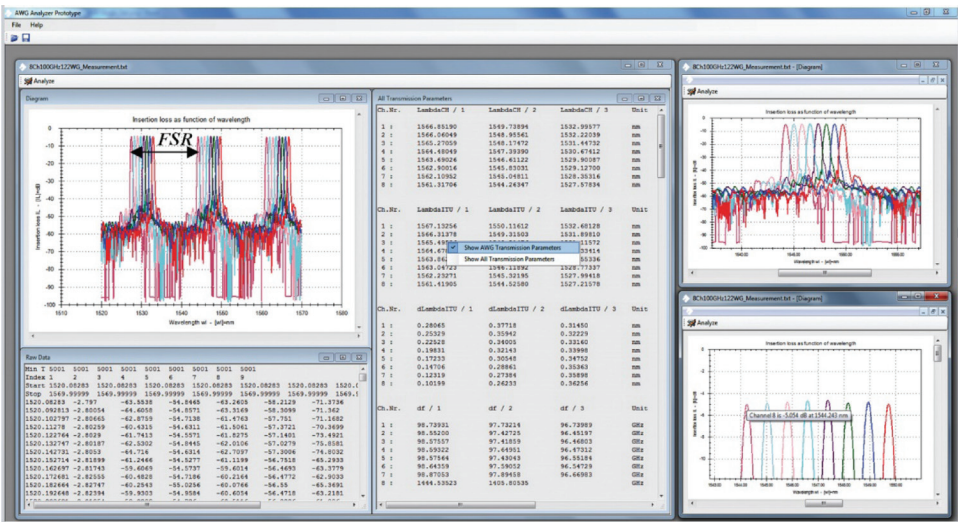

Figure 26 Multiple spectrum transmission characteristics of an 8-channel, 100-GHz AWG (consisting of multiple orders of the PA response with a *FSR*).

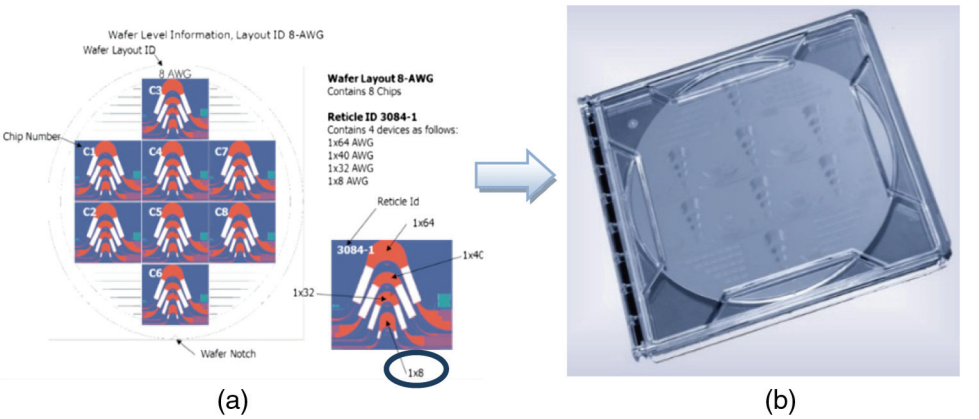

Figure 27 Mask layout consisting of various AWG designs including the 8-channel, (a) 100-GHz AWG and (b) fabricated 8" wafer.[67]

- **AWG tutorial:** For teaching purposes, a tutorial about AWGs including functionality, AWG types, design, fabrication, testing, and packaging is implemented in the tool.

3.6 Technological verification of AWG design

Once the AWG designs are completed and ready for fabrication, the next step is to export these designs (usually in GDSII format). From all of the individual GDSII files, a complete mask layout will be generated and sent to a mask house for production. Figure 27(a) shows the final mask layout with different AWGs including the 8-channel, 100-GHz AWG designed here. Once produced, the mask will later be used in the lithography process to transfer the AWG structures onto the wafer.

3.6.1 Fabrication

From a technological point of view, a silica AWG is a planar waveguide structure usually fabricated on a silicon wafer with SiO_2 lower-cladding oxide obtained by such means using thermal oxidation of an Si substrate (having refractive index n_{cl}). The chemical vapor deposition (CVD) process creates a Ge-doped SiO_2 active layer (core layer) with a refractive index, n_c, higher than the refractive index of the cladding layer. Optical lithography and dry etching then define the AWG waveguide structure. The growth of the upper cladding (CVD process) with a refractive index matching the lower cladding is the last fabrication step (Fig. 28). The fabricated wafer is shown in Fig. 27(b).

3.6.2 Measurement

The fabricated chips must first be diced and can then be measured on a wafer level (Fig. 29). The measurement method used by most AWG vendors is the

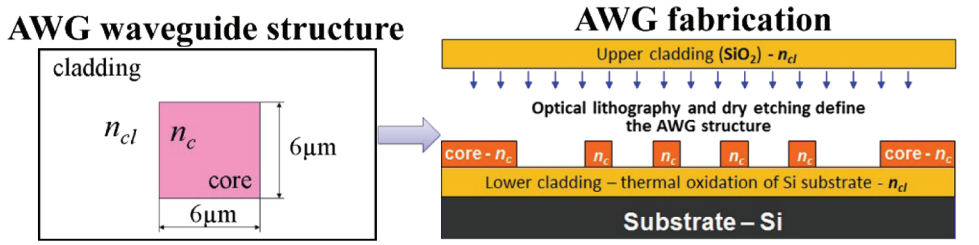

Figure 28 AWG fabrication.

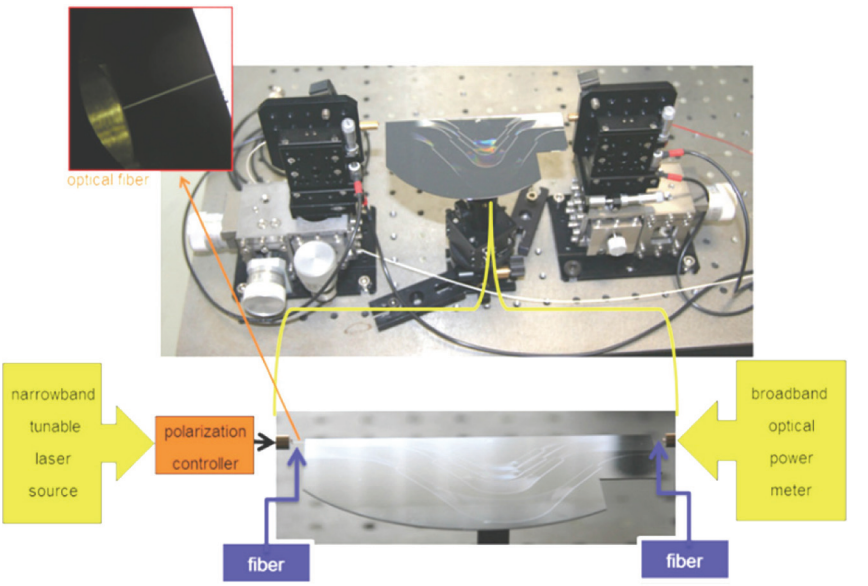

Figure 29 AWG measurement setup.[88]

so-called Mueller matrix method.[83] For this purpose, the polarization controller is used to set the known polarization state at input before light enters the AWG structure. The measurement over the required spectral range is realized by a narrowband tunable laser source that sends the desired optical wavelengths into the input waveguide through the fiber. After the light has traveled through the AWG, the broadband optical power meter, connected via fiber to one of the output waveguides, measures the output optical power. The measurement is performed for each output channel in the whole spectral range. The output of these measurements once again forms the transmission characteristics.

3.6.3 Evaluation of measured transmission characteristics

Figure 30 shows simulated transmission characteristics from Fig. 15 together with the measured transmission characteristics of the designed and fabricated

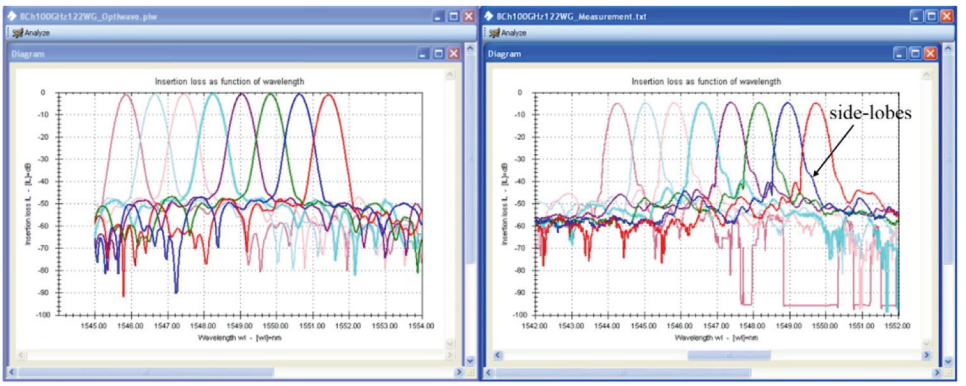

Figure 30 (a) Simulated and (b) measured transmission characteristics of the 8-channel, 100-GHz AWG.

8-channel, 100-GHz AWG. As can be seen, there is a close correlation between them, which is also confirmed by the transmission parameters calculated from both simulated and measured characteristics using the AWG-Analyzer tool (Table 2).

Table 2 shows the most important transmission parameters, namely the input parameters (input for the AWG-Parameters tool) and the parameters calculated from simulated and measured transmission characteristics (output from the AWG-Analyzer tool). As shown, the AWG central wavelengths λ_c from simulated and measured transmission characteristics do not agree with the designed value *Lambda* = 1550.12 nm. This deviation is a result of the effective refractive index used in the Optiwave tool, whose calculated value does not match the technology. Insertion loss calculated within the passband (25% of channel spacing) $IL = -2.624$ dB. Measured insertion loss reached $IL = -6.438$ dB. This parameter is always higher than its simulated value as it also includes the coupling losses between the fibers and waveguides, and propagation losses in the AWG structure. Insertion loss uniformity L_u (design) and *ILu* (simulation and measurement) is similar in all three cases because this parameter depends primarily on the far-field intensity in the output star coupler, as presented in Fig. 12(a). Here, the small deviations result from the slightly different spectral responses. The AWG-Parameters tool calculates with the ideal Gaussian shape, while the simulated and measured non-uniformity also depend on the tapers used in the AWG design (Section 3.10). These tapers form the Gaussian shape and thus influence some transmission parameters. For adjacent channel crosstalk *Cr* (design) and *AX* (simulation and measurement) a strong correlation can be seen between the theoretical value ($Cr = -29.33894$ dB) and the measurement ($AX = -32.476$ dB). The simulated value ($AX = -42.024$ dB) is approximately 10 dB better than the channel crosstalk calculated from the measured characteristics. This difference results

Table 2 Input parameters used in the 8-channel, 100-GHz AWG design (AWG-Parameters tool) together with parameters calculated from the simulated transmission characteristics (AWG-Analyzer tool: simulation) and from the measured transmission characteristics (AWG-Analyzer tool: measurement).

Transmission parameters	AWG-Parameters tool: input parameters	AWG-Analyzer tool: simulation	AWG-Analyzer tool: measurement
No. of channels	*Num* = 8	*Nr. Channels* = 8	*Nr. Channels* = 8
AWG central wavelength (λ_c)	*Lambda* = 1550.012 nm	λ_c = 1549.00 nm	λ_c = 1547.50 nm
Channel spacing	*df* = 100 GHz	*Ch. Spacing* = 100 GHz	*Ch. Spacing* = 100 GHz
Insertion loss		*IL* = −2.624 dB	*IL* = −6.438 dB
Insertion loss uniformity	*Lu* = 0.712248 dB	*ILu* = 0.520 dB	*ILu* = 0.694 dB
Adjacent channel crosstalk	*Cr* = −29.338942 dB	*AX* = −42.024 dB	*AX* = −32.476 dB
Non-adjacent channel crosstalk		*nAX* = −46.413 dB	*nAX* = −46.308 dB
Background crosstalk		*BX* = −54.571 dB	*BX* = −54.793 dB

from the side lobes in the measured characteristics [shown in Fig. 30(b)], which originated from fabrication imperfections. For both non-adjacent channel crosstalk *nAX* and background crosstalk *BX*, there is also a very strong correlation between the simulated and measured values.

3.7 Thermal control

In order to use AWG devices in practical optical-communication applications, precise wavelength control and long-term wavelength stability are needed. If the temperature of an AWG fluctuates, the channel wavelength will naturally change according to the thermal coefficient of the material used. By making use of the thermo-optic effect, a temperature controller can be built into the AWG package to control and tune the device to the ITU grid or any other desired wavelength.

However, various companies have already demonstrated the use of athermal AWGs.[89,90] This principle involves using a special silicon resin in part of the lightwave circuit that has a temperature coefficient different from that of quartz glass.[91–93] This design cuts the temperature dependence of the wavelengths to less than one-tenth of its original value, which makes using a temperature-control device unnecessary.

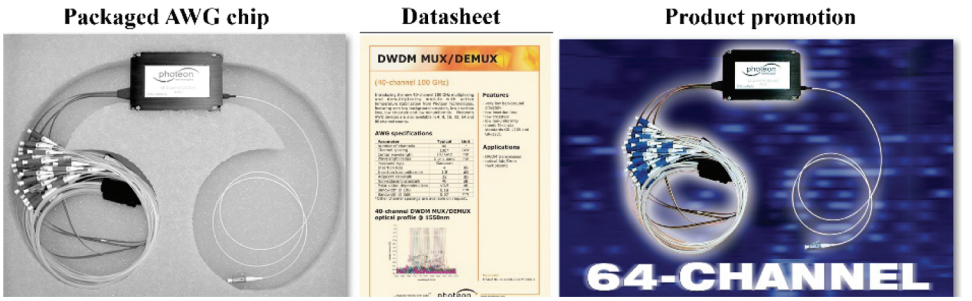

Figure 31 Packaged AWG chip, datasheet, and product promotion.[67]

3.8 Packaging and product promotion

After the transmission parameters (calculated from the measured transmission characteristics) reach the required values, the fabricated AWG chip can be packaged [see Fig. 31(a)] and tested under a defined set of temperature and environmental conditions.[94] Only such packaged chips can be used in real optical networks. Each AWG is delivered with a datasheet including the most important information about the product [Fig. 31(b)]. Product promotion is the final step in the AWG production line [Fig. 31(c)].[95]

3.9 Different photonics tools

There are various photonic tools commercially available on the market for the design and simulation of AWGs. Although the design procedures are very similar, the simulation results obtained can vary greatly from one tool to another. Therefore, optical design companies prefer to develop their own photonic design tools. In this section, we present the simulation and evaluation of the 8-channel, 100-GHz AWG described here using three commercially available software tools (Apollo Photonics, Optiwave, and RSoft). For this purpose, the identical waveguide structure, described in Fig. 7(a), was first created using all three photonic tools. Then the AWG geometrical parameters [output from the AWG-Parameters tool, Fig. 17(b)] were used to create the AWG layout. For all simulations, the same calculation conditions were used. The simulated transmission characteristics together with the measured transmission characteristics are shown in Fig. 32. From the transmission characteristics, it is evident that the simulation performed by the Optiwave tool is very similar to the measurement. The simulated characteristics from Apollo Photonics and from RSoft are similar to each other, but they differ slightly from the measured characteristics. They feature much better background isolation (*BX*).

All transmission characteristics were evaluated using the AWG-Analyzer tool. Table 3 shows the transmission parameters calculated from the transmission characteristics in Fig. 32. As can be seen again, the AWG central wavelength λ_c only

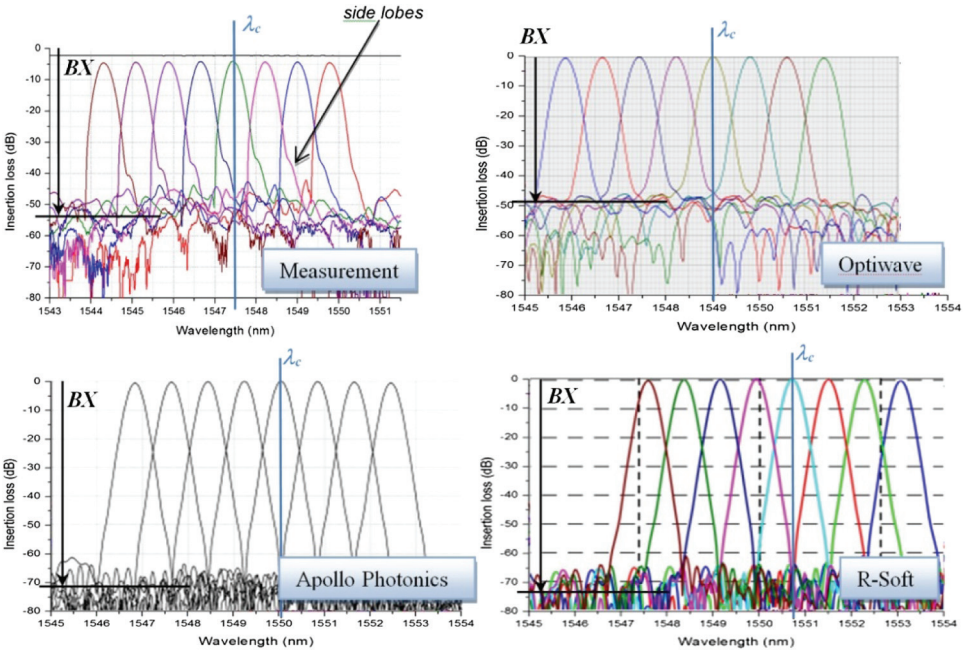

Figure 32 Simulated transmission characteristics from three different photonics tools and from the measured transmission characteristics of the simulated and fabricated 8-channel, 100-GHz AWG.[96]

Table 3 Transmission parameters calculated from the measured and simulated transmission characteristics (Optiwave, Apollo Photonics, RSoft).

Transmission parameters	Measurement	Optiwave	Apollo	RSoft
AWG central wavelength (λ_c)	1547.50 nm	1549.00 nm	1550.12 nm	1550.70 nm
Insertion loss (*IL*)	–6.438 dB	–2.624 dB	–2.306 dB	–2.000 dB
Insertion loss uniformity (*ILu*)	0.694 dB	0.520 dB	0.760 dB	0.529 dB
Adjacent channel crosstalk (*AX*)	–32.476 dB	–42.024 dB	–50.426 dB	–50.264 dB
Non-adjacent channel crosstalk (*nAX*)	–46.308 dB	–46.413 dB	–65.438 dB	–63.032 dB
Background crosstalk (*BX*)	–54.793 dB	–54.571 dB	–71.050 dB	–73.309 dB

correlates with the designed value λ_c = 1550.12 nm in the Apollo simulation. The deviations resulting with the other two tools (RSoft and Optiwave) are caused by the effective refractive index, whose calculated value is slightly different in each photonic tool. Insertion loss *IL*, calculated within the passband (25% of channel spacing), is similar for all simulations and lies between −2 dB (RSoft) and −2.624 dB (Optiwave). The small deviations result only from the slightly different Gaussian shapes. The measured insertion loss reached −6.438 dB. Insertion loss uniformity *ILu* is similar in all simulations and in the measurement because this parameter depends mainly on the AWG structure itself (the far-field intensity in the output star coupler). Here again, the small deviations result from the slightly different Gaussian shapes. Adjacent channel crosstalk *AX* (also calculated within the passband) is very similar for Apollo and RSoft characteristics (about −50 dB) because their characteristics are nearly identical. Adjacent crosstalk from the Optiwave simulation equals −42.024 dB and is approximately 10 dB better than the adjacent channel crosstalk calculated from the measured characteristics (−32.476 dB). As already mentioned, this difference is a result of the side lobes in the measured characteristics, originating from fabrication imperfections. Non-adjacent channel crosstalk *nAX* and background crosstalk *BX* show the same tendency, i.e., a very strong correlation between the measurement and Optiwave simulation, and between the Apollo and RSoft simulations.

In summary, the calculated transmission parameters show very similar results, although the closest correlation was achieved between the measurement and the Optiwave simulation. It should be noted, however, that the Apollo and RSoft tools perform much faster BPM simulations than the Optiwave tool. The simulation of an 8-channel, 100-GHz AWG, e.g., takes just a few hours when using the Apollo or RSoft tool but between 1 and 2 days with the Optiwave tool. On the other hand, the Optiwave tool features a user-friendly interface and also partially supports the calculations of AWG geometrical parameters (so can be used to design AWGs with some design limitations) and the calculation of some transmission parameters.

3.10 Tapers in AWG design

As described in Section 3.9, the small deviations between the calculated transmission parameters from various simulated transmission characteristics (Fig. 32) are the result of different simulation approaches used in different photonics tools. These different approaches cause variations in the Gaussian spectral response, despite the fact that the same AWG is being simulated in each case. However, of greater importance for practical use are the deviations between the transmission parameters calculated from simulated and measured characteristics. The variation in spectral response is caused primarily by the application of tapers in the AWG design. However, the AWG-Parameters tool (used to design the AWG and thus also to calculate the AWG geometrical parameters)

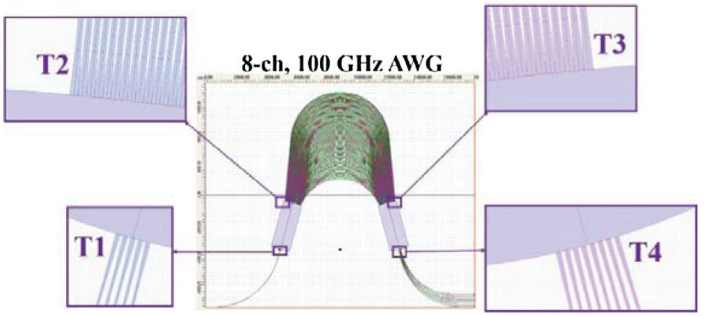

Figure 33 Different tapers used in AWG design.

does not allow for any tapers in AWG design (Section 3.3, model of Smit and van Dam).

Tapers can be placed at four different positions in the AWG layout (Fig. 33):

- T1 tapers connect the input waveguide with the input star coupler.
- T2 tapers connect the input star coupler with the PA waveguides.
- T3 tapers connect the PA waveguides with the output star coupler.
- T4 tapers connect the output star coupler with the output waveguides.

If the AWG is intended as both a MUX and DeMUX, then the tapers are usually designed symmetrically, i.e., T1 taper = T4 taper and T2 taper = T3 taper. However, different tapers can be used depending on the application. In order to demonstrate their effect on the AWG's performance, we used the same 8-channel, 100-GHz AWG design and performed various simulations of the AWG layout, first with no tapers, then with the application of T1 linear taper, then once each with T2 linear tapers, T3 linear tapers, and T4 linear tapers, as shown in Fig. 33. Figure 34 shows the simulated spectral response in each case. Although it can be seen that the responses are very similar to one another, Table 4 shows the calculated transmission parameters from all characteristics in Fig. 34 that feature some deviations resulting from the application of different tapers that fulfill different functions in the design.

Influence of taper T1: Taper T1 is placed in front of the input star coupler and may have a range of different shapes, as presented in Fig. 35, such as linear taper, multimode interference (MMI) coupler or parabolic waveguide horn taper, etc. These tapers form the spectral response of the AWG, i.e., Gaussian shape, flat-top shape, or semiflat.[60] The spectral response when applying the linear taper can be seen in Fig. 34(b), the MMI taper in Fig. 8(b), and the parabolic taper in Fig. 8(c). As is evident in Fig. 35, the near-field intensities leaving the taper and entering the input star coupler correlate well with the spectral responses of the AWG. This correlation is due to the fact that the PA can be seen as an extended lens, in which the input field at the object plane of the input star coupler is transferred to an equal field on the focal line of the output star coupler (Fig. 5).

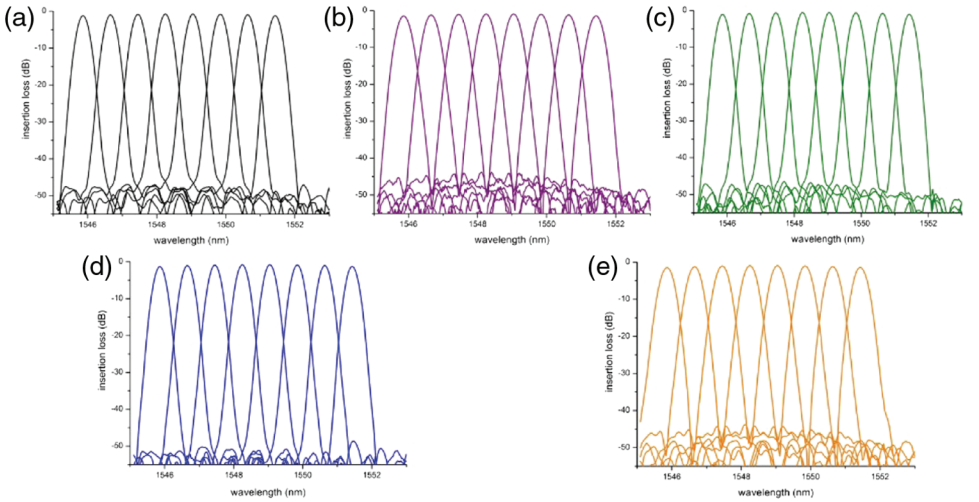

Figure 34 Simulated transmission characteristics of an 8-channel, 100-GHz AWG applying different tapers: (a) no tapers, (b) linear taper T1, (c) linear taper T2, (d) linear taper T3, and (e) linear taper T4.

Table 4 Transmission parameters calculated from AWG designs in Fig. 34. Values in bold are the best values reached, while those in italics represent the worst case.

Transmission parameters	**AWG design (no taper)**	**AWG design (taper T1)**	**AWG design (taper T2)**	**AWG design (taper T3)**	**AWG design (taper T4)**
Insert. loss (*IL*) (dB)	*−2.58*	−2.5	**−2.36**	*−2.58*	−2.5
Insertion loss uniform. (*ILu*) (dB)	**0.5**	0.54	**0.5**	*0.62*	0.54
Adjacent channel crosstalk (*AX*) (dB)	−43.10	*−36.09*	−42.93	**−46.64**	*−36.48*
Nonadjacent channel crosstalk (*nAX*) (dB)	**−46.97**	*−44.67*	**−47.06**	**−46.88**	*−44.79*
Background crosstalk (*BX*) (dB)	**−56.367**	*−48.11*	−54.62	−53.38	*−47.9*

The resulting spectral response can then be derived from a superposition of the imaged field at the focal line and the eigenmode of the output waveguide.

Influence of taper T2: Linear tapers connecting the input star coupler with the PA waveguides are used to reduce losses when light enters the array aperture. This loss occurs due to reflection of the light at the facets of the interspaces

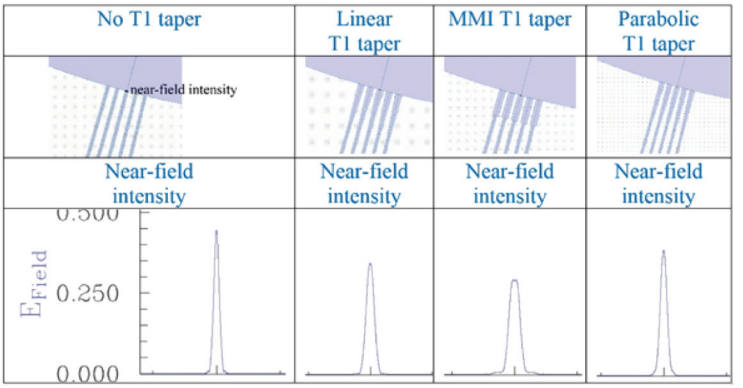

Figure 35 Different T1 tapers used in AWG design to form the spectral response.

between the individual PA waveguides. Light penetrating the cladding material at these facets is usually absorbed. This loss can be minimized by maintaining only a small distance between the array waveguides or by adding linear tapers.[97]

Influence of taper T3: Linear tapers connecting the PA waveguides with the output star coupler influence the far-field intensity distribution in this coupler and thus determine the non-uniformity parameter L_u [Fig. 12(a)].

Influence of taper T4: Tapers used at the end of the output star coupler fulfill two different functions. They can be used in a similar manner as taper T1 to form the spectral response of the AWG[60] or to collect the light focused at the focal line into the output waveguides. On the one hand, losses can thus be reduced, but on the other hand, the adjacent channel crosstalk increases because a part of the light can also be focused into the neighboring waveguides (discussed in Section 3.3 AWG design, "channel crosstalk").

Based on the functionalities of various tapers in the AWG design, we can draw the following conclusions. As can be seen in Fig. 36(a), the transmission

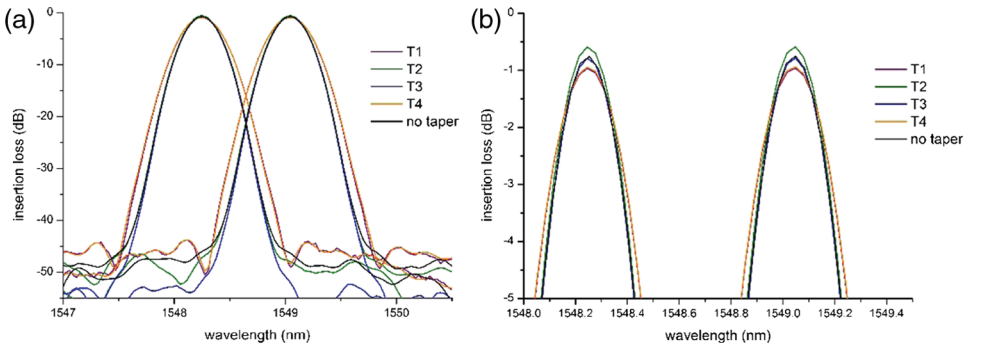

Figure 36 (a) Transmission characteristics of two center channels from all five simulated transmission characteristics presented in Fig. 34, and (b) a detailed view of insertion losses.

characteristics that result from application of the linear tapers T1 and T4 (which have the same dimensions) are quite similar to one another. They form the wider Gaussian shape, which correlates well with the near-field intensity from the linear taper that is wider than the near-field intensity resulting when no tapers are used in the AWG design (Fig. 35). Transmission characteristics when applying linear tapers T2 and T3 are nearly identical to the transmission characteristics when no taper is used in the AWG design. They feature a narrower Gaussian shape ensuring better crosstalk (*AX*, *nAX*, *BX*) as presented in Table 4. Small deviations between these parameters are the result of numerical approximations in the transmission parameter's calculations. As was to be expected, the lowest insertion loss, *IL* (calculated within the passband), was achieved by applying taper T2 [Fig. 36(b)]. The worst non-uniformity (*ILu*) resulted from the application of taper T3. The wider this taper is, the narrower the far-field intensity in the output star coupler, i.e., the higher the non-uniformity.

3.11 Influence of fabrication imperfections on AWG performance

Passive optical components, such as AWGs, splitters, ring resonators, and photonic crystals, are very sensitive to fabrication imperfections. Even though the AWG may be well designed, the fabrication process will greatly influence the end performance of the AWG. Among the various imperfections that may occur during fabrication are as follows:

- **Material imperfections:** These result from inhomogeneous doping over the wafer (inhomogeneous refractive index of the core, cladding) that stems from the CVD deposition process.
- **Size imperfections:** The waveguide structure may not have the correct size, which will influence the light traveling through the waveguides. Incorrect height stems from the CVD growth, while incorrect width of the waveguide results mainly from the lithography and etching processes.

The performance of the AWG may fluctuate greatly depending on which foundry is used, despite the fact they may offer the same technology for fabrication. Furthermore, even AWGs produced in the same technological run or from the same fabricated wafer may vary in performance.

3.11.1 Different foundries

Although most of the foundries offer the same (or very similar) fabrication processes, the performance of fabricated chips can vary greatly from one to the other. Figure 37 shows the performance fluctuation of a 40-channel, 100-GHz AWG coming from different technological foundries.

This AWG was designed, simulated, and evaluated using the same procedure as described for the 8-channel, 100-GHz AWG. As can be seen, each of the measured transmission characteristics is different, and they are sorted in such a way

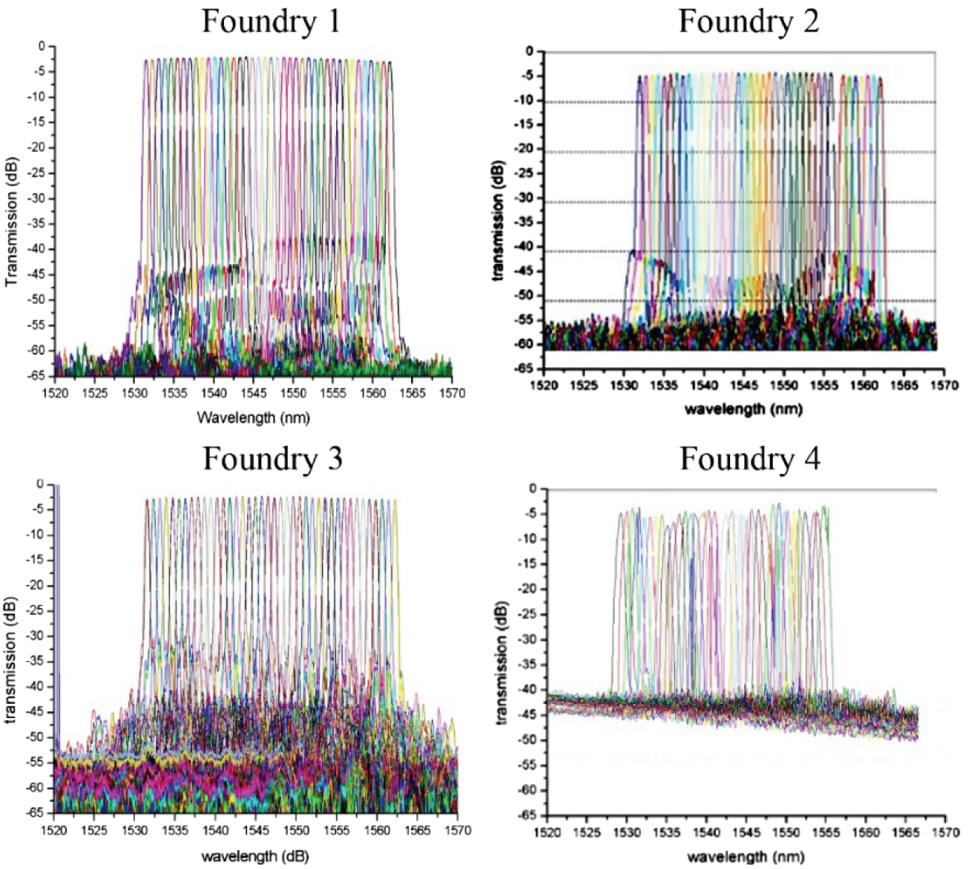

Figure 37 Measured transmission characteristics of a 40-channel, 100-GHz AWG from four different foundries.[67]

that foundry 1 displays the best performance and each of the next foundries demonstrates a successively worse AWG performance. Of particular note are the background crosstalk and channel crosstalk, which are both considerably higher. Channel crosstalk is a result of the phase errors caused by variations in the effective length of the array grating arms due to fabrication imperfections or wafer non-uniformity (Section 3.3 AWG design, "Channel crosstalk"). The phase errors result in wide fuzzy focus spots on the focal line (Fig. 5). When the output waveguides are placed too close to one another (input design parameter *dx* in Fig. 16), a part of the optical signal may also be focused into the neighboring waveguides, increasing the adjacent channel crosstalk *AX*. From the design point of view, in order to minimize channel crosstalk, the PA waveguides should, therefore, be as short as possible (parameter *dL*), and output waveguides should be placed as far as possible from each other (parameter *dx*).

3.11.2 Different AWG performances from the same foundry

Figure 38 shows the same 40-channel, 100-GHz AWG as in Fig. 37 but on five different wafers each from foundry 1 and foundry 3. As can be seen, the result of foundry 1's fabrication process is superior to that of foundry 3. The 40-channel, 100-GHz AWG from foundry 1 features not only excellent measured transmission characteristics, confirmed by the calculated transmission parameters (Table 5), but these are also very similar, which ensures very good technological reproducibility.

In contrast to this result, the same AWG fabricated in foundry 3 displays not only great variation in transmission characteristics from different wafers, but also far worse transmission characteristics than those of foundry 1. This AWG will be described more in detail.

3.11.3 40-channel, 100-GHz AWG

The AWG-Parameters tool was used to design a 40-channel, 100-GHz AWG. From the calculated geometrical parameters (i.e., *dx*, *dd*, *Lf*, and *dL*), an AWG layout was created and simulated using the Apollo Photonics tool. Figure 39 shows the simulated and measured transmission characteristics of this AWG, which show close parity. Using the AWG-Analyzer tool, the transmission parameters were calculated from both the simulated and measured transmission characteristics and then evaluated [Figs. 40(a) and 40(b)]. Table 5 presents the calculated transmission parameters: the design parameters (AWG-Parameters tool) and the transmission parameters calculated from the simulated and measured transmission characteristics (AWG-Analyzer tool). As this AWG comes from the same design and technological run as the 8-channel, 100-GHz AWG, there is a slight shift in the measured AWG central wavelength (λ_c = 1548.35 nm) in comparison to the designed and simulated central wavelength ($\lambda_c \sim$ 1550.12 nm). The parameter peak insertion loss uniformity *pILu* is very similar in all three cases (design: L_u = 0.982 dB, simulation: *pILu* = 0.873 dB, and measurement: *pILu* = 0.754 dB). Small deviations are merely the result of slightly different optical signal shapes. Other transmission parameters, such as adjacent channel crosstalk, non-adjacent channel crosstalk, and background crosstalk, also show a strong correlation, which once again confirms the computational correctness of the AWG-Parameters and AWG-Analyzer tools, as well as the high quality of foundry fabrication facilities.

3.12 Application of AWG tools in various AWG designs

The tools described above were applied to various AWG designs.[67,98] Most of them were designed to have Gaussian and flat-top shapes, although some designs had a semiflat spectral response. Depending on the application, some AWGs required a special design. Those AWGs will be presented in this section.

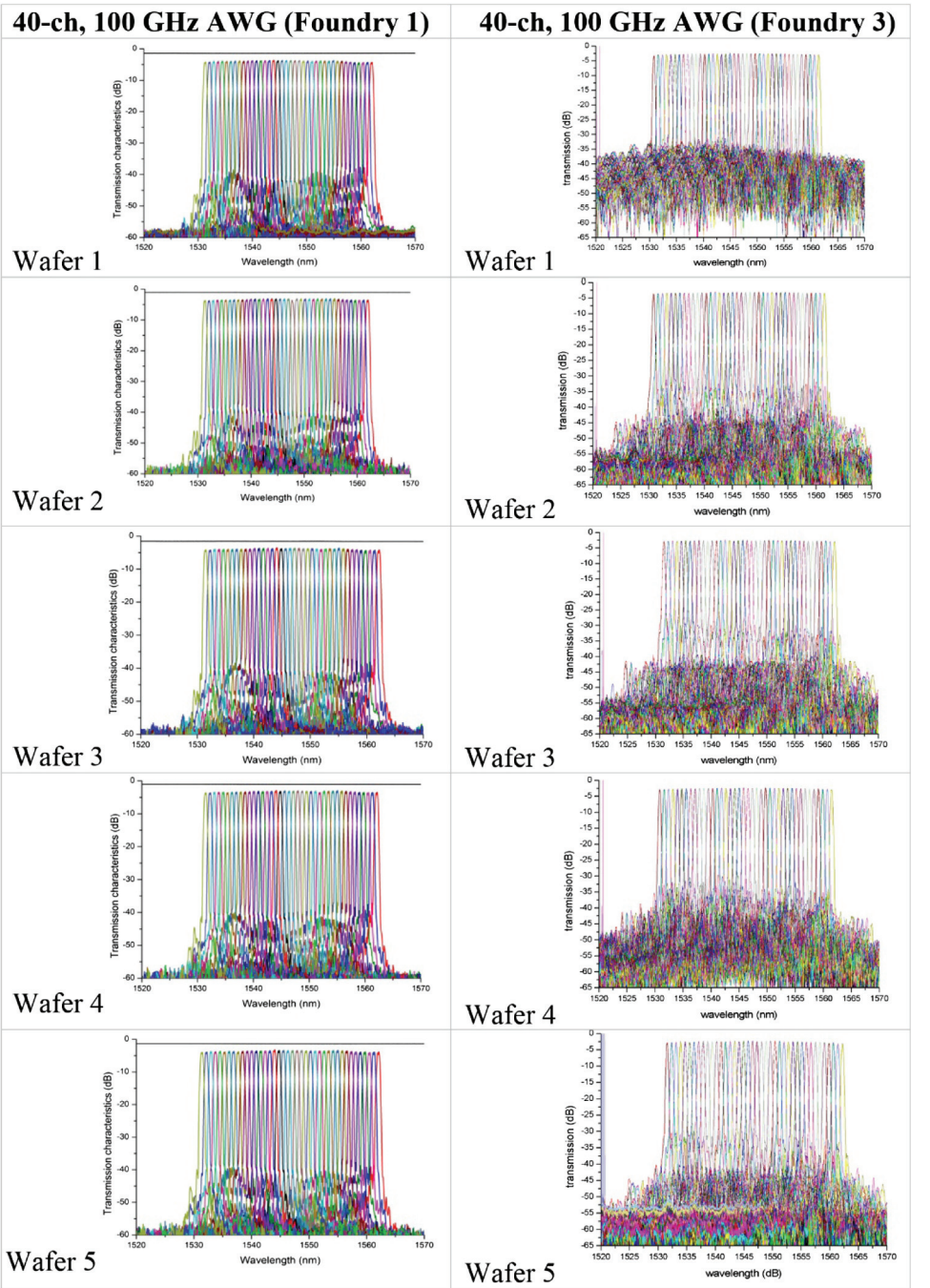

Figure 38 Measured transmission characteristics of a 40-channel, 100-GHz AWG (foundry 1 and foundry 3) from five different wafers.[67]

Table 5 Input design parameters used in the 40-channel, 100-GHz AWG design (AWG-Parameters tool) together with parameters calculated from the simulated transmission characteristics (AWG-Analyzer tool: simulation) and from the measured transmission characteristics (AWG-Analyzer tool: measurement).

Transmission parameters	AWG-Parameters tool: input parameters	AWG-Analyzer tool: simulation	AWG-Analyzer tool: measurement
No. of channels	*Num* = 40	*Nr. Channels* = 40	*Nr. Channels* = 40
AWG central wavelength	λ_c = 1550.043 nm	λ_c = 1550.12 nm	λ_c = 1548.35 nm
Peak insertion loss		*pIL* = –1.502 dB	*pIL* = –4.145 dB
Insertion loss		*IL* = –2.833 dB	*IL* = –5.964 dB
Peak insertion loss uniformity	*Lu* = 0.982 dB	*pILu* = 0.873 dB	*pILu* = 0.754 dB
Insertion loss uniformity		*ILu* = 0.923 dB	*ILu* = 0.785 dB
Adjacent channel crosstalk	*Cr* = –31.4 dB	*AX* = –30.395 dB	*AX* = –30.280 dB
Non-adjacent channel crosstalk		*nAX* = –37.703 dB	*nAX* = –40.664 dB
Background crosstalk		*BX* = –65.197 dB	*BX* = –67.631 dB

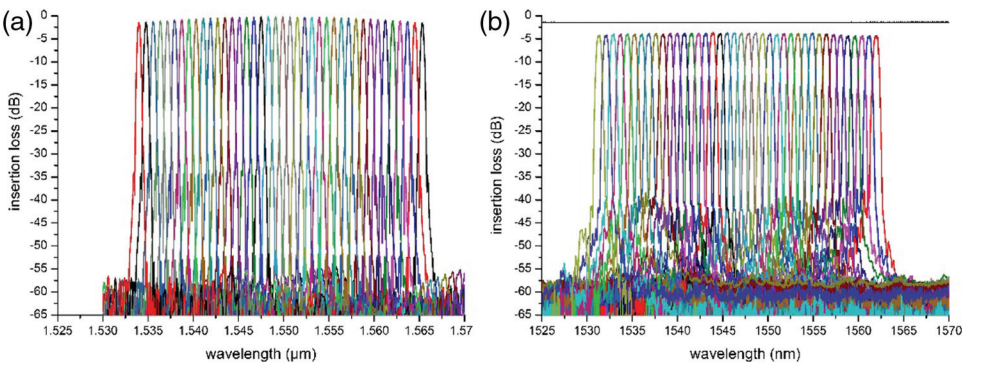

Figure 39 40-channel, 100-GHz AWG: (a) simulated transmission characteristics from Apollo Photonics and (b) measured transmission characteristics.

3.12.1 8-channel CWDM AWG

The 8-channel CWDM AWG has a typical channel spacing *df* = 2500 GHz (= 20 nm) and a spectral response with a flat-top shape. Depending on which part of the AWG structure is modified, different approaches can be used to form the flat-top AWG spectral response.[60]

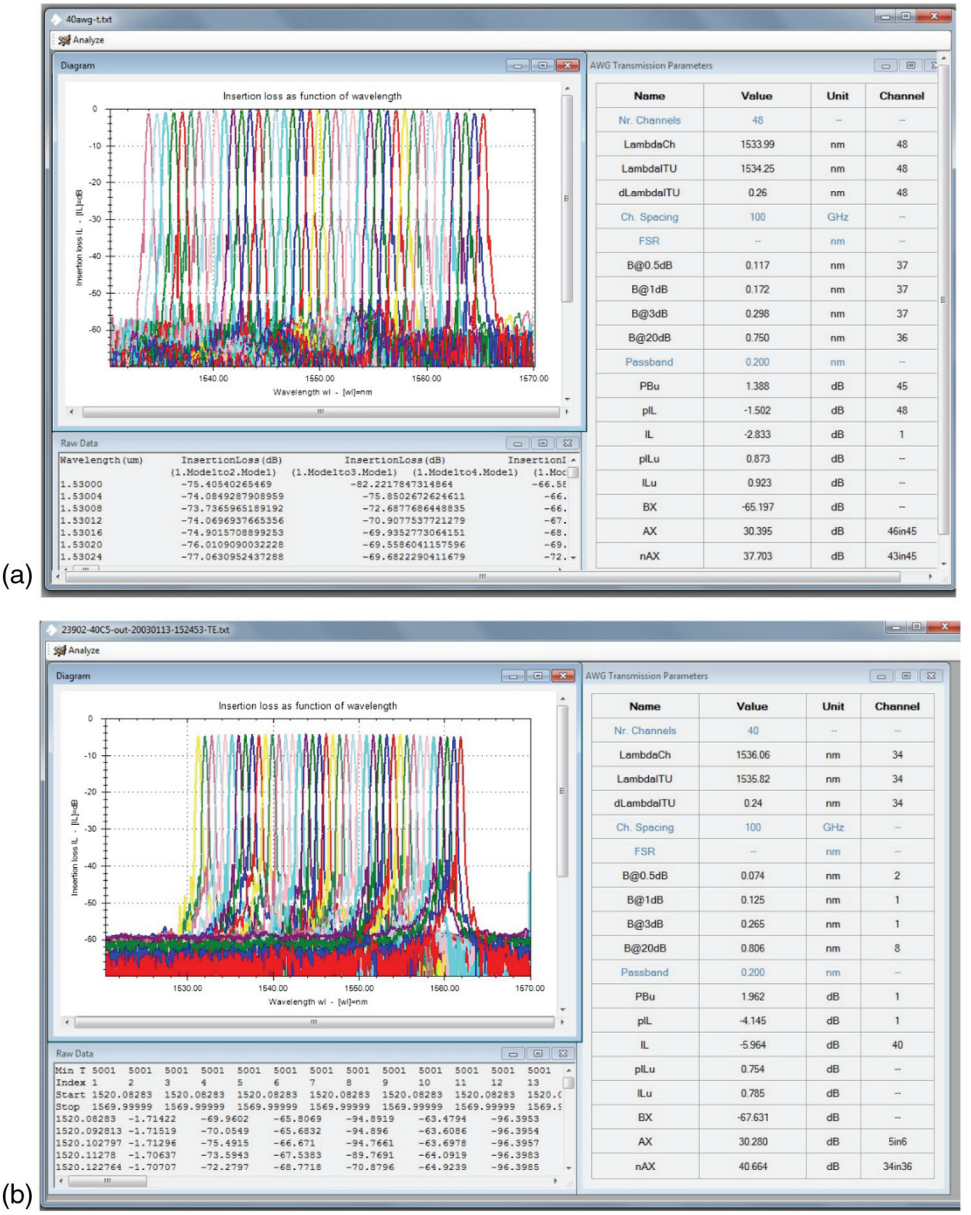

Figure 40 40-channel, 100-GHz AWG: calculated transmission parameters from the simulated transmission characteristics (a) and from the measured transmission characteristics (b) using the AWG-Analyzer tool.

Input section modification (multimode input waveguides) involves flattening the passband by connecting the input waveguide with the input star coupler by means of a special taper, such as a MMI coupler,[99] parabolic waveguide horn,[100] or Y-branch.[101] In all three cases, the principle of flattening is the same.

The special tapers applied will form the flat-top near-field intensity at the object plane of the input star coupler, which is imaged to an equal field at the image plane of the output star coupler (Section 3.10 Tapers in AWG design).

The star-coupler-modification approach (two focal points for the waveguide gratings) is based on the principle whereby the array waveguide region is split into two or more different groups, each of which focuses to slightly different focal points.[102] The displacement of the individual focal points is in the range of a few microns. The resulting field on the image plane is a superposition of the different Gaussian responses leading to a broadened response peak with a flattened top shape.

The grating section modification approach (multiple grating sections) uses two or more different gratings,[103] each with its own path length difference ΔL and individual center wavelength. Once again, the resulting spectral response is a superposition of two slightly displaced Gaussian peaks.

Output section modifications [post-filtering with asymmetric Mach–Zehnder interferometers (MZIs)] is a method based on subsequent filtering of the output signals with a MZI.[104] The round peaks of the Gaussian channel response are flattened by the MZI filters, which have the opposite spectral characteristics of the individual WDM channels.

Output section modification (multimode output waveguides) involves modification of the output waveguides. A part of each output waveguide is spread to a MMI coupler that connects the output star coupler[105] (Section 3.10 Tapers in AWG design).

All of these approaches have certain advantages and disadvantages. Based on Ref. 60, the most simple but also most effective solution is the use of input waveguide modification that was also applied to the 8-channel CWDM AWG.

3.12.2 Design

The design of CWDM AWGs is made difficult by the fact that the wide channel spacing (df = 2500 GHz) leads to a very small length difference between two neighboring PA waveguides dL. Such a small length difference causes difficulties in connecting all the waveguides in the PA. On the other hand, a small dL leads to a very large bending radius of waveguides, which in turn reduces the propagation losses (Fig. 41).

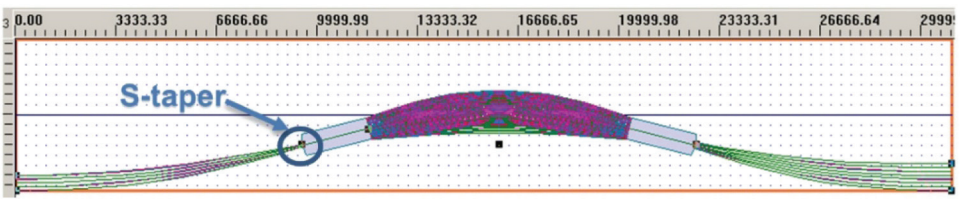

Figure 41 Top view of the 8-channel CWDM AWG layout (Optiwave tool).

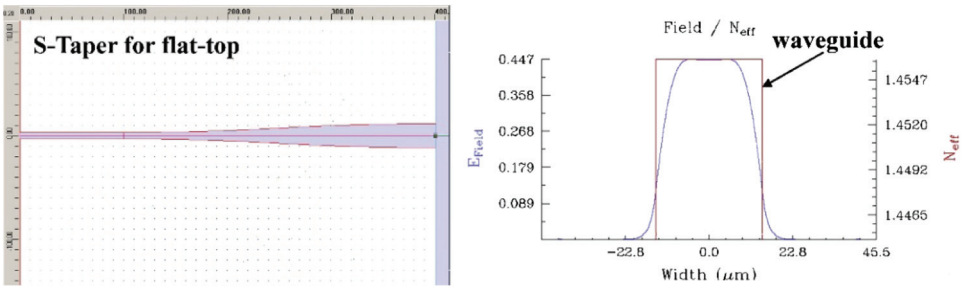

Figure 42 (a) Top view of the S-taper used in designing the 8-channel CWDM AWG to form the flat-top, (b) with the field intensity distribution at the taper output.

For the flat-top shape, an S-taper (a parabolic waveguide horn) as predefined in the photonic software was used in the AWG layout. This taper shape is often used to form the flat-top shape because it ensures highly satisfactory results (as shown in Fig. 42, Optiwave simulation).

Figure 43 shows the (a) simulated and (b) part of the measured transmission characteristics of this AWG. While the simulated spectral response demonstrates a shape close to semiflat, the shape of the measured spectral response correlates strongly with the designed shape, as shown in Fig. 42(b).

Table 6 presents the designed transmission parameters calculated using the AWG-Parameters tool, the transmission parameters calculated from the simulated and measured transmission characteristics presented in Fig. 43.

Insertion loss: The CWDM AWG suffers far higher insertion losses because of the flat-top shape. As can be seen, the simulated peak insertion loss pIL reached -4.9 dB, and the measured peak insertion loss $pIL = -6.12$ dB. The

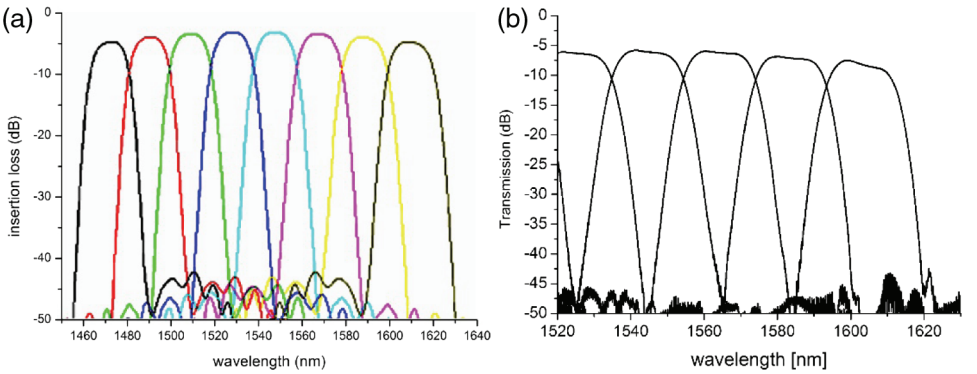

Figure 43 8-channel CWDM AWG: (a) simulated and (b) measured transmission characteristics.[67]

Table 6 Input parameters used in the CWDM 8-channel, 2500-GHz AWG design (AWG-Parameters tool) together with parameters calculated from the simulated and measured transmission characteristics (AWG-Analyzer tool).

Transmission parameters	AWG-Parameters tool: input parameters	AWG-Analyzer tool: simulation	AWG-Analyzer tool: measurement
No. of channels	*Num* = 8	*Nr. Channels* = 8	*Nr. Channels* = 8
AWG central wavelength	λ_c = 1550.12 nm	λ_c = 1550.12 nm	λ_c = 1547 nm
Peak insertion loss		*pIL* = –4.9 dB	*pIL* = –6.12 dB
Insertion loss		*IL* = –7.43 dB	*IL* = –9.122 dB
Peak insertion loss uniformity	*Lu* = 1.9 dB	*pILu* = 2.043 dB	*pILu* = 2.134 dB
Insertion loss uniformity		*ILu* = 2.21 dB	*ILu* = 2.19 dB
Adjacent channel crosstalk	*Cr* = –39.8 dB	*AX* = –32.45 dB	*AX* = –30.12 dB
Non-adjacent channel crosstalk		*nAX* = –43.620 dB	*nAX* = –39.551 dB
Background crosstalk		*BX* = –53.428 dB	*BX* = –51.781 dB

insertion loss *IL* is even higher: from the simulation, *IL* = −7.43 dB, and from the measurement, *IL* = −9.122 dB.

Insertion loss uniformity (non-uniformity): The theoretical value of the non-uniformity used in the AWG-Parameters tool was set to L_u = 1.9, while the simulated and measured non-uniformity reached values below 2.2 dB. These values demonstrate a strong correlation between all three parameters. Once again, the small deviations result from the slightly different shapes of the spectral responses. Insertion loss uniformity *IL* also features very good agreement between simulated and measured values.

Adjacent channel crosstalk: The designed adjacent crosstalk was set to *Cr* = −39.8 dB. Its simulated and measured values are similar to one another (about −30 dB), but they differ strongly from this theoretical value because of the flat-top shape of the output signals formed by applying the S-taper. This taper forms much wider output signals, causing higher adjacent channel crosstalk. The AWG-Parameters tool does not allow for tapers used to form the flat-top shape of the optical signal, but it calculates the value of the channel crosstalk as for a Gaussian shape.

Non-adjacent channel crosstalk: The simulated non-adjacent channel crosstalk is slightly better than the non-adjacent channel crosstalk calculated from the

measured transmission characteristics, as was the case for the other AWGs coming from this technological run (foundry 3).

Background crosstalk: The two background crosstalk values are similar.

3.12.3 Colorless 8-channel, 100-GHz AWG

The AWG-Parameters tool was applied to design various AWG optical MUX/DeMUX. In this section, some additional features of this tool for designing an 8-channel, 100-GHz colorless AWG are presented. When a special design is applied, such an AWG will repeat its orders and can work in any predefined channel band. In other words, the same colorless AWG can work on channels 1 to 8 or 9 to 16, and so on, as shown in Fig. 9(b). In the frequency domain, this period is called the FSR, as shown in Fig. 12(b). The condition for a colorless AWG is that the FSR should equal *Num* times channel spacing, where *Num* is the number of output channels. In our case, $FSR = 8 \times 100$ GHz = 800 GHz. In the AWG-Parameters tool, it can be easily calculated using the parameter *dfsr*, as shown in Fig. 44 in the "Computed data" window (containing all additive parameters needed for the calculation).

3.12.3.1 Layout and simulation

The geometrical parameters calculated using the AWG-Parameters tool (Fig. 44) create the input for the layout of the 8-channel, 100-GHz colorless AWG. This

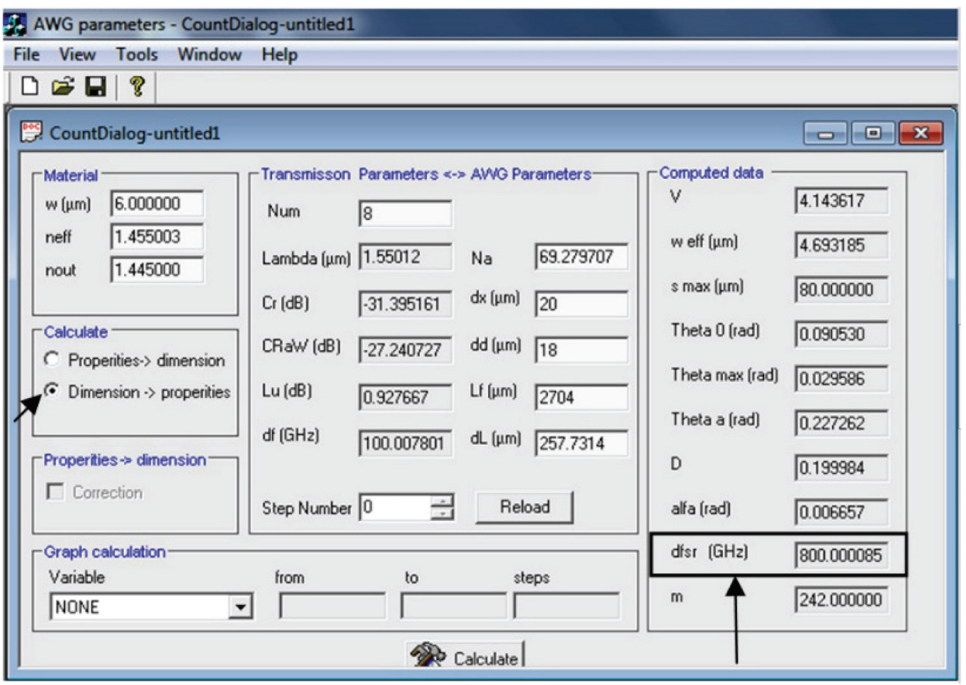

Figure 44 Calculated geometrical parameters of the 8-channel, 100-GHz colorless AWG.

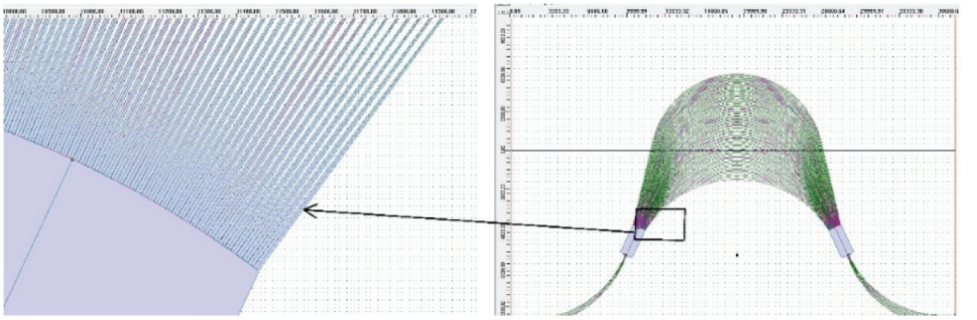

(a) (b)

Figure 45 Colorless 8-channel, 100-GHz AWG layout with linear tapers used in the PA to collect the light and thus reduce the coupling losses between the PA waveguides and input star coupler.

layout was created and simulated using the Optiwave photonics tool [Fig. 45(b)]. The simulated transmission characteristics are presented in Fig. 46(a). The design was also verified technologically, and the measured transmission characteristics are shown in Fig. 46(b). As can be seen, very good correlation was achieved between simulated and measured transmission characteristics, with the exception of background crosstalk that is approximately 10 dB higher in the measured transmission characteristics,[106] as also confirmed by the calculated transmission parameter *BX* in Table 7.

Insertion loss: Higher insertion loss than for the other Gaussian AWGs is caused mainly by much higher non-uniformity.

Insertion loss uniformity (non-uniformity): The simulated and measured non-uniformity parameters *pILu* are similar to each other; however, they deviate strongly from their theoretical value L_u. The reason for this deviation is the large waveguide separation between the PA waveguides (parameter *dd* = 18 μm, Fig. 44).

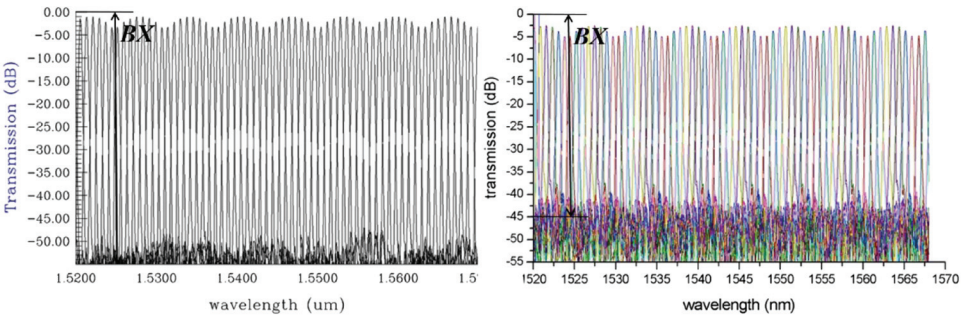

(a) (b)

Figure 46 (a) Simulated and (b) measured transmission characteristics of the 8-channel, 100-GHz colorless AWG.[67]

Table 7 Input parameters used in the colorless 8-channel, 100-GHz AWG design (AWG-Parameters tool) together with parameters calculated from the simulated and measured transmission characteristics (AWG-Analyzer tool).

Transmission parameters	AWG-Parameters: input parameters	AWG-Analyzer: simulation	AWG-Analyzer: measurement	AWG-Analyzer: simulation (no T3 used)
Insertion loss		IL = –4.76 dB	IL = –6.12 dB	IL = –6.38 dB
Peak insertion loss uniformity	Lu = 0.927 dB	$pILu$ = 2.38 dB	$pILu$ = 2.4 dB	$pILu$ = 1.09 dB
Adjacent channel crosstalk	Cr = –31.395 dB	AX = –33.1 dB	AX = –32.8 dB	AX = –35.4 dB
Non-adjacent channel crosstalk		nAX = –47.2 dB	nAX = –37.5 dB	nAX = –47.7 dB
Background crosstalk		BX = –55 dB	BX = –45 dB	BX = –57 dB

To reduce the transition losses between the star couplers and arrayed waveguides (Section 3.3 AWG design, "Performance parameters"—"Insertion loss"), linear tapers (T2 taper = T3 taper) were used in the PA to collect the light [Fig. 45(a)]. From the Fourier transform, it follows that the wider these tapers are, the narrower the far-field intensity in the output star coupler, which in turn negatively affects the non-uniformity parameter L_u (Section 3.10 Tapers in AWG design—"Influence of taper T3"). Unfortunately, the application of tapers in the PA is not possible in the AWG structure calculation or in the AWG-Parameters tool. However, the presence of the tapers in the designed and fabricated AWG structure is evidenced by the very good agreement between the simulated (2.38 dB) and measured non-uniformity (2.4 dB).

Adjacent channel crosstalk: There is only a small deviation in adjacent channel crosstalk (Cr) caused by the slightly different shapes of the optical signals in the simulated and measured transmission characteristics (AX).

Non-adjacent crosstalk and background crosstalk: The channel isolation from the simulated characteristics is approximately 10 dB better than the measured channel isolation.

The example of an 8-channel, 100-GHz colorless AWG is ideal for demonstrating the application of theory in the design process. If this AWG is designed to work solely as a DeMUX, there is no need to use the symmetrical tapers in the PA. If taper T3 is removed from the AWG design, the far-field intensity should correlate with the peak insertion loss uniformity L_u (Table 7). Figures 47 and 48 confirm this theory. Figure 47 shows simulations of the far-field intensity

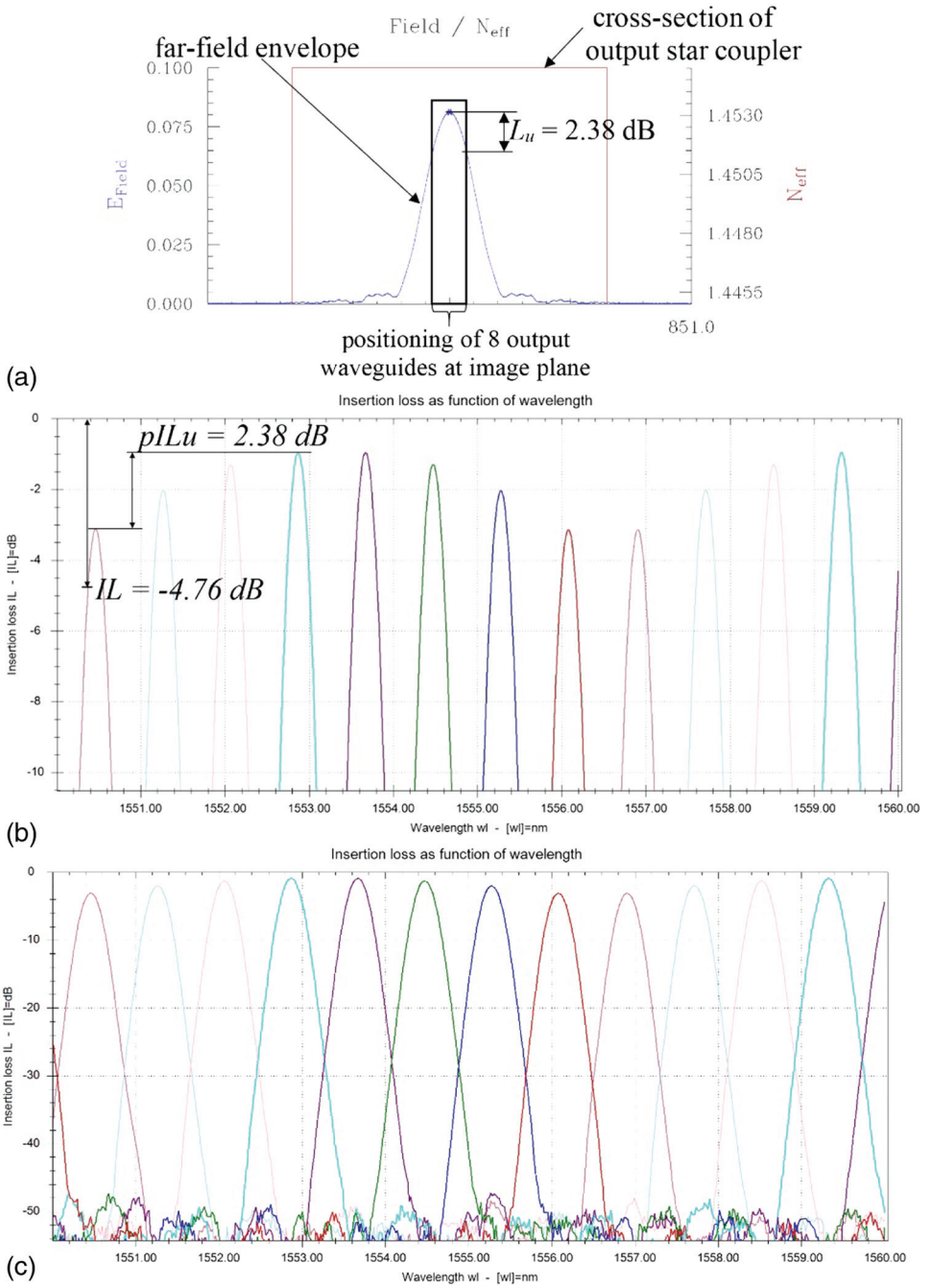

Figure 47 (a) Simulated far-field intensity in the output star coupler, (b) the non-uniformity parameter, and (c) transmission characteristics of the 8-channel, 100-GHz colorless AWG when taper T3 was used.

in the output star coupler, the non-uniformity parameter, and the transmission characteristics (in the wavelength range of 1550 to 1560 nm) from the colorless AWG when taper T3 was used.

Figure 48 shows the same simulations but without application of the T3 taper. The far-field intensity explains very clearly why the non-uniformity *pILu* is much lower when the T3 taper is not used, but the final losses of the AWG are much higher (parameter $IL = -6.38$ dB). This fact is confirmed by the calculated transmission parameters in Table 7. From this, it follows that when an appropriate taper T3 is used in the AWG design, it may form a far-field envelope that can strongly reduce the insertion loss non-uniformity.[107]

3.12.4 128-channel, 10-GHz AWG for ultra-DWDM

In recent years, the optical MUX/DeMUX based on AWGs have also become increasingly popular for very high dense wavelength division multiplexing applications.[108,109] This popularity is largely due to the fact that the AWGs offer many advantages, such as precisely controlled narrow-channel spacing (easily matched to the ITU grid), simple and accurate wavelength stabilization, low and uniform insertion loss, and large channel counts. To date, a number of narrow-channel-spacing AWGs (10 GHz, 25 GHz) with channel counts of 400 or even more have already been demonstrated;[29,30,110] however, they do not reach the transmitting characteristics required for data transmission in future optical networks. The reason is that although the standard-channel-count (up to 40) and standard-channel-spacing (100 or 50 GHz) AWGs feature very good transmission characteristics and are relatively easy to design, increasing the channel counts (128 or more) and narrowing the channel spacing (25 GHz, 12.5 GHz, 10 GHz, or even less) lead to a rapid increase in the AWG size which, in turn, causes deterioration in optical performance with higher insertion loss and, in particular, higher channel crosstalk.[59] Therefore, the design of such AWGs is very complicated and requires special knowledge in this field. The simulations of such large AWGs are also accompanied by a huge computational effort (one simulation takes from weeks to months), with the result that these AWGs present a serious challenge for the designers.

In this section, the 128-channel 10-GHz AWG will be described. The AWG structure was designed using the AWG-Parameters tool, simulated using the Optiwave tool, and evaluated using the AWG-Analyzer tool. The simulation of the AWG structure took approximately two months when using the Optiwave tool. The simulated transmission characteristics can be seen in Fig. 49, which shows the transmission parameters of all 128 output channels. Figure 50 shows the transmission characteristics of just one output channel.

The simulated transmission characteristics were then evaluated using the AWG-Analyzer tool (Fig. 51). The designed transmission parameters from the AWG-Parameters tool were a peak insertion loss uniformity $L_u = 0.938754$ dB and a channel crosstalk between output waveguides $Cr = -29.329885$ dB.[111]

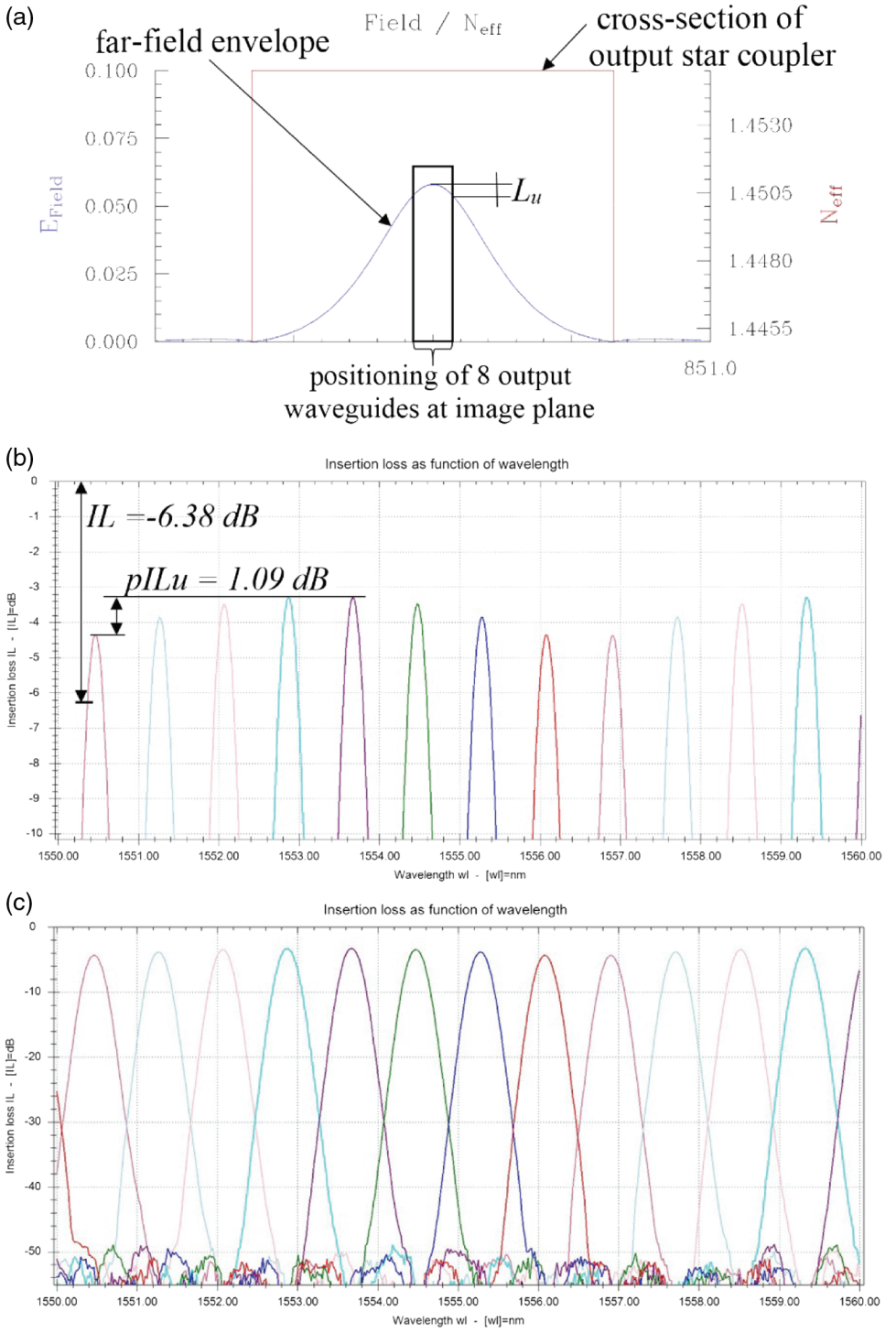

Figure 48 (a) Simulated far-field intensity in the output star coupler, (b) the nonuniformity parameter, and (c) transmission characteristics of the 8-channel, 100-GHz colorless AWG without taper T3.

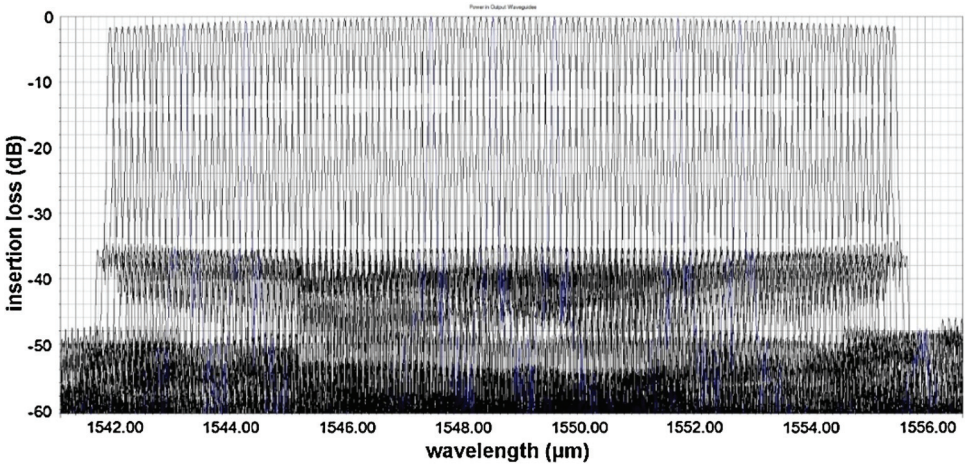

Figure 49 Simulated transmission characteristics of the 128-channel, 10-GHz AWG obtained from the Optiwave photonics tool.

The transmission parameters calculated from simulated transmission characteristics (Fig. 51) are an insertion loss parameter $pIL = -1.339$ dB and an insertion loss parameter calculated within the passband $IL = -2.271$ dB. All of the other calculated transmission parameters also feature very good values: adjacent channel crosstalk $AX = -28{,}692$ dB, non-adjacent channel crosstalk $nAX = -32.947$ dB, and background crosstalk $BX = -65.701$ dB (the BX parameter can be seen in Fig. 50 where only one optical transmitting signal is presented). The

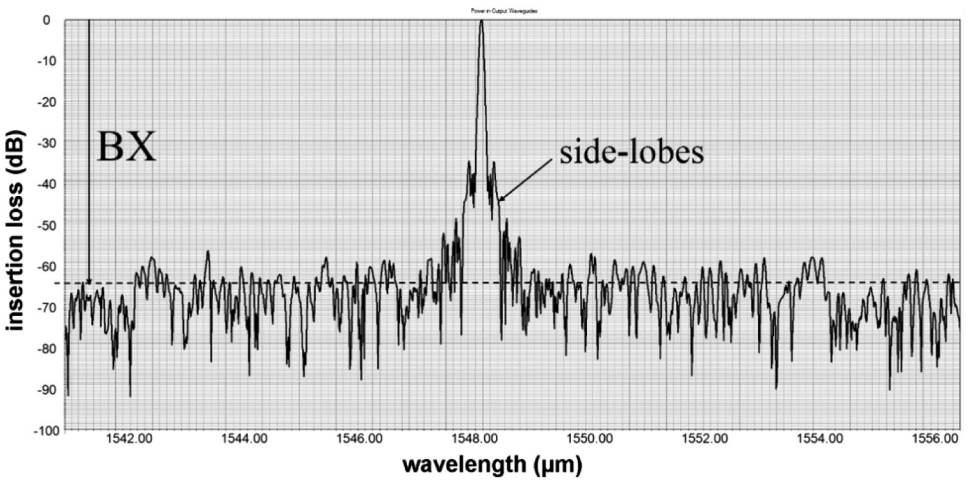

Figure 50 Simulated transmission characteristics of only one channel from the 128-channel, 10-GHz AWG.

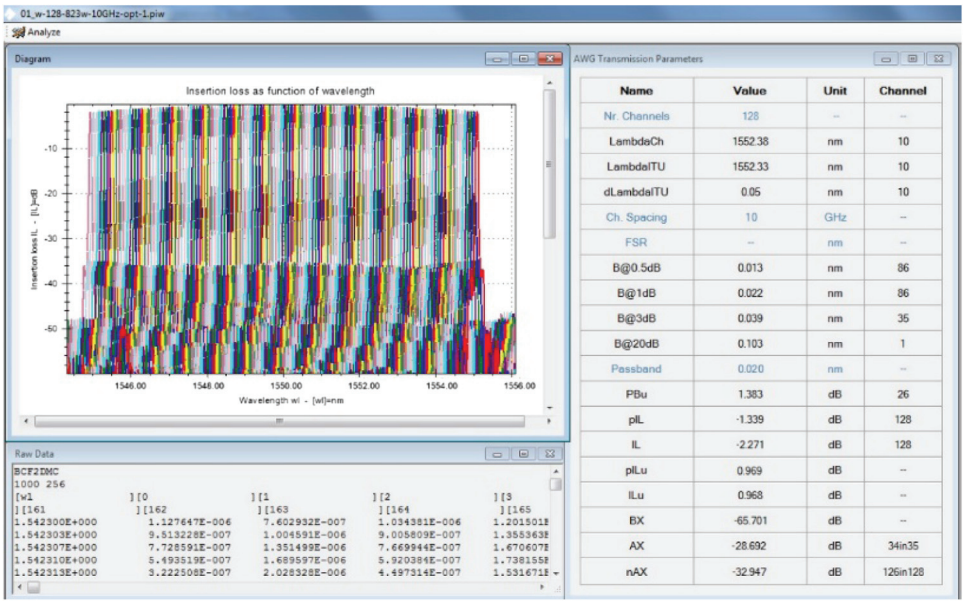

Name	Value	Unit	Channel
Nr. Channels	128	--	--
LambdaCh	1552.38	nm	10
LambdaITU	1552.33	nm	10
dLambdaITU	0.05	nm	10
Ch. Spacing	10	GHz	--
FSR	--	nm	--
B@0.5dB	0.013	nm	86
B@1dB	0.022	nm	86
B@3dB	0.039	nm	35
B@20dB	0.103	nm	1
Passband	0.020	nm	--
PBu	1.383	dB	26
pIL	-1.339	dB	128
IL	-2.271	dB	128
pILu	0.969	dB	--
ILu	0.968	dB	--
BX	-65.701	dB	--
AX	-28.692	dB	34in35
nAX	-32.947	dB	126in128

Figure 51 Calculated transmission parameters from the simulated transmission characteristics presented in Fig. 49.

big difference between the channel crosstalk and background crosstalk is caused by the presence of the side-lobes.

The final AWG structure fits on a 6-in. wafer, as presented in Fig. 52.

3.13 Design optimization

An optical MUX/DeMUX based on an AWG is an attractive optical device, which offers a great deal of flexibility in the design. As already shown, certain input parameters are needed to calculate the geometrical parameters of the AWG structure. By simply changing these parameters, it is then possible to design various AWGs with very satisfying performances. Sometimes, and particularly for high-channel-count and narrow-channel-spacing AWGs, defining the input parameters is not a satisfactory approach due to other issues, such as the size of the AWG structure or fabrication, which determine the final performance of the AWG. In this case, it is necessary to look for new solutions.

3.13.1 Improvement of channel crosstalk in narrow-channel-spacing AWGs by applying specially shaped couplers

As explained in the design of the 128-channel, 10-GHz AWG, the high-channel-count and narrow-channel-spacing AWGs are very large in size, causing an accumulation of phase errors in the grating arms that leads to a deterioration in the optical performance, and in particular a marked increase in channel crosstalk.

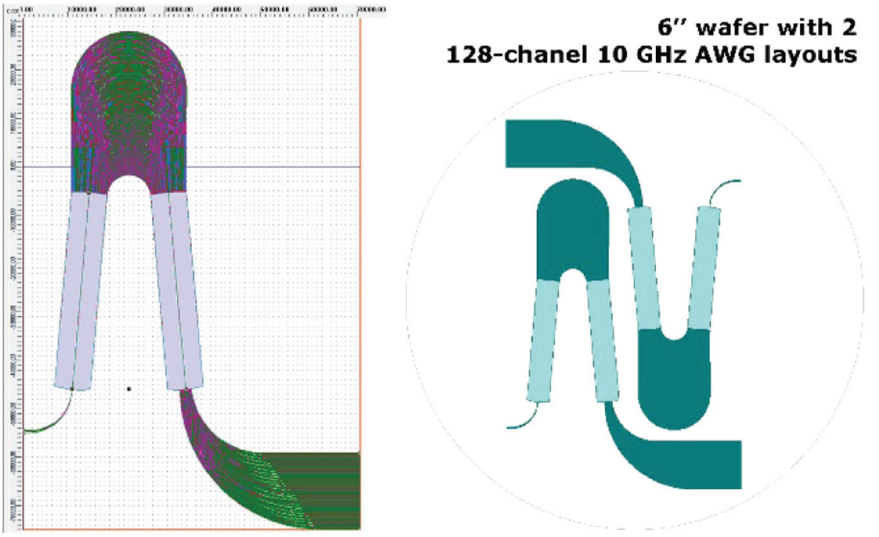

Figure 52 (a) Layout of the 128-channel, 10-GHz AWG and (b) layout of two 128-channel, 10-GHz AWGs placed on a 6-in. wafer.

Channel crosstalk is not only the result of phase errors but also the amplitude errors in the far-field intensity at the end of the input star coupler.[59] To minimize the phase errors, the arrayed waveguides should be designed to be as short in length as possible. On the other hand, short arrayed waveguides lead to an increase in the star coupler size, causing an increase in amplitude errors. Therefore, it is a difficult task to design and fabricate an AWG with both narrow channel spacing and low channel crosstalk, and even AWGs with 25-GHz channel spacing present a serious challenge. One solution is specially shaped couplers, which, in combination with the short length of arrayed waveguides, can minimize both the phase errors as well as amplitude errors, and thus allow for considerable improvement in the channel crosstalk.[112] For the purposes of showing the influence of the coupler shape on the AWG's optical performance, a standard and also optimized 25-GHz AWG with $Num = 256$ output waveguides was designed. The number of PA waveguides was set to 1000, and the optical path length difference between adjacent waveguides $dL = 23.5$ μm. The layout of this AWG, featuring a small PA region in comparison to the large star couplers, is shown in Fig. 53.

For the standard AWG design, the "standard" coupler shape was used, and for the optimized AWG, the "specially shaped" couplers (Fig. 54).

3.13.2 Simulation of a standard AWG

To minimize the phase errors in the standard AWG, the path length difference of the adjacent arrayed waveguides dL was set to a low value ($dL = 23.5$ μm). The

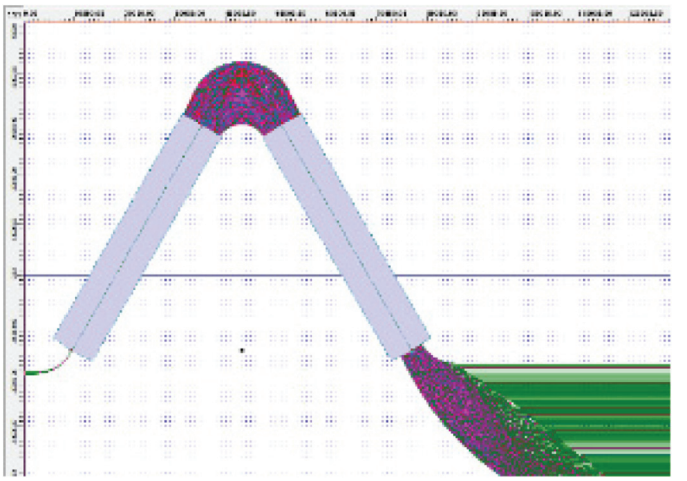

Figure 53 256-channel, 25-GHz AWG layout, (10 × 13) cm^2 in size.

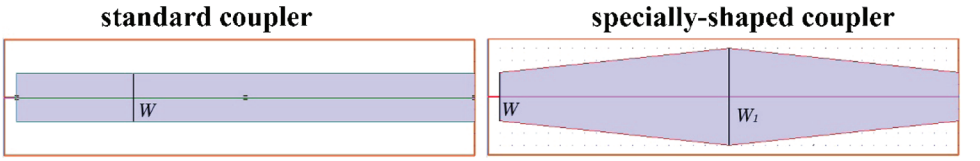

Figure 54 The shapes of AWG couplers: standard and specially shaped couplers used in the design of a 256-channel, 25-GHz AWG.

amplitude errors were minimized by setting the appropriate width of the couplers, $W = 7000$ μm according to the width of the far-field intensity, as shown in Fig. 55(a). However, as can be seen, the far-field intensity at the end of the input star coupler still displays strong amplitude irregularities causing the high channel crosstalk. Figure 55(b) shows the simulated transmission characteristics of this AWG (of the first 39 channels only because of the enormous computing time needed for the calculations). Calculated channel crosstalk $AX \sim -24$ dB, insertion loss $IL < -35$ dB, and background crosstalk $BX \sim -52$ dB.

3.13.3 Simulation of an optimized AWG

To eliminate amplitude errors, the specially shaped star couplers presented in Fig. 54(b) were used. These couplers led to an alteration in the far-field intensity, which became smoother [Fig. 56(a)], and this in turn had a positive influence on the transmission characteristics, as shown in Fig. 56(b). The calculated channel crosstalk $AX \sim -28$ dB, insertion loss $IL < -3.3$ dB, and background crosstalk $BX \sim -62$ dB.

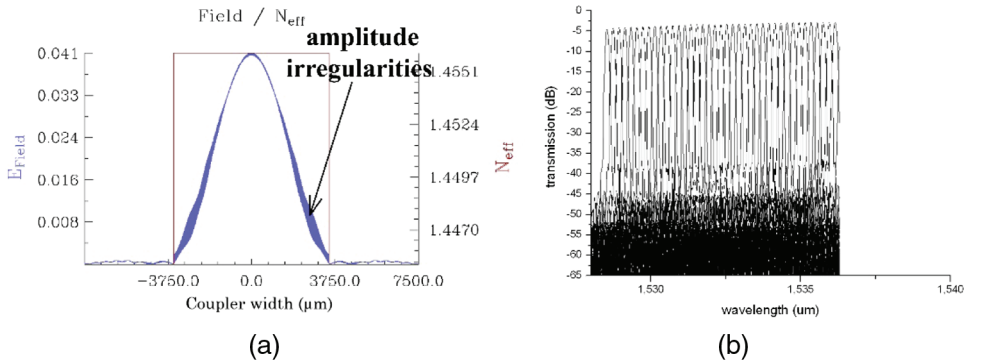

Figure 55 (a) Far-field intensity at the end of the input star coupler (b) together with simulated transmission characteristics.

3.13.4 Design of specially shaped couplers

As presented, the specially shaped couplers suggested here can be used to reduce the channel crosstalk in narrow-channel-spacing AWGs. From a geometrical point of view, the couplers have the same length as standard couplers but only have the same width W at the beginning and end of the coupler (Fig. 54). This value increases toward the middle of the coupler where it reaches its maximum value W_1 and then falls again to the original value W. Thus, W_1 is the only variable parameter that must be determined. It corresponds to any point where the far-field intensity distribution at the end of the standard input star coupler reaches its zero value outside the coupler (Fig. 57). In this design, W_1 = 15,000 µm, but W_1 = 9000 µm also produced very satisfactory results.

We found various coupler shapes to be effective. Of these different shapes, the greatest improvement in channel crosstalk was obtained for the coupler presented in the right half of Fig. 54. Figure 58 clearly shows the significant

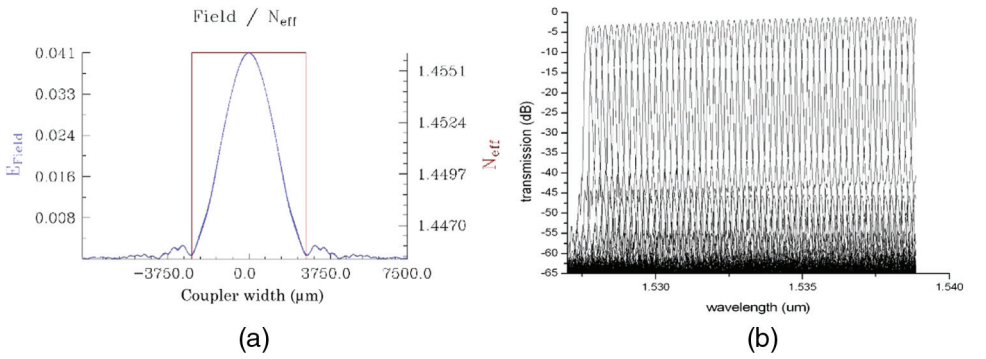

Figure 56 (a) Alteration to the far-field intensity by applying specially shaped couplers, (b) with simulated transmission characteristics.

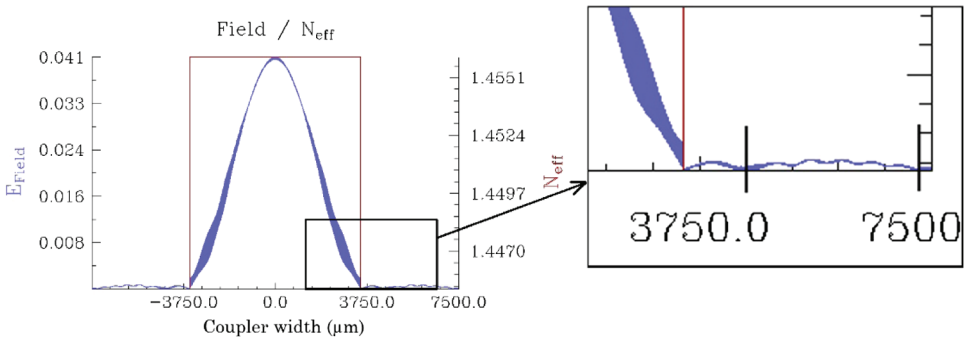

Figure 57 Far-field intensity distribution at the end of the standard input star coupler with its zero points outside the coupler.

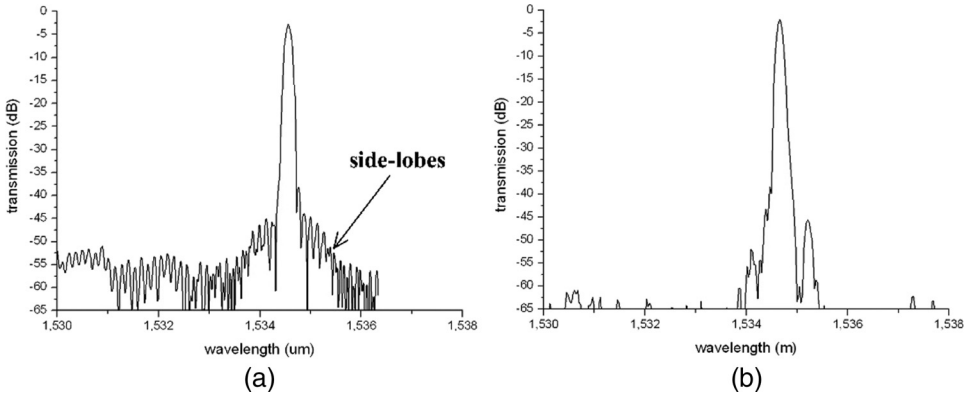

Figure 58 (a) Transmission characteristics of one channel using standard couplers and (b) specially shaped couplers.

influence of such specially shaped couplers on the AWG's optical performance, where we plotted AWG transmission characteristics from Fig. 55(b) and from Fig. 56(b) again, but only for one channel. As can be seen, the output optical signal from the standard AWG (a) features high side-lobes causing high crosstalk between the output channels; and (b) the specially shaped couplers led to the elimination of amplitude errors at the output aperture of the input star coupler with a strong impact on the AWG transmission characteristics. The side lobes of the optical signal are strongly suppressed, leading to a significant improvement in channel crosstalk. In particular, the background crosstalk was reduced by ∼10 dB.

The approach of using specially shaped couplers to reduce channel crosstalk has a number of advantages. First, it is not sensitive to small shape and size deviations caused by possible process variations during the fabrication, as the couplers are very large compared to the other AWG parts, nor does it have a negative

Table 8 Comparison of transmission parameters calculated from transmission characteristics of standard and specially shaped 256-chanel, 25-GHz AWGs.

Transmission parameters	Standard couplers	Specially shaped couplers
Insertion loss (*IL*)	−3.5 dB	−3.3 dB
Adjacent crosstalk (*AX*)	−24 dB	−28 dB
Nonadjacent crosstalk (*nAX*)	−45 dB	−50 dB
Background crosstalk (*BX*)	−52 dB	−62 dB

effect on other transmission parameters, such as non-uniformity or insertion loss. It also led to the slight improvement of insertion loss presented in Table 8 and allows for the use of specially shaped couplers in combination with any tapers or other special structures placed at the waveguides.

Acknowledgments

My sincere thanks go to my family, who has been my greatest support during all this time, and, in particular, to my husband, Heinz Seyringer, who deserves a very special mention for his invaluable assistance in helping me realize this work. Thanks also go to my Master's students, who spent long hours poring over solutions for scientific tasks with me and preparing scientific articles and conference presentations.

References

1. www.lightriver.com.
2. ITU-T Recommendation G.694.1, "Spectral grids for WDM applications: DWDM frequency grid," (2012).
3. Y. A. Yudin and C. A. Armiento, "Trends in DWDM multiplexers and their impact on network performance," *Lightwave Online* (2003).
4. J. J. Pan, F. Q. Zhou, and M. Zhou, "Thin films improve 50-GHz DWDM devices," *Laser Focus World* **38**, 111 (2002).
5. G. H. Abdullah, B. R. Mhdi, and N. A. Aljaber, "Design thin film narrow band-pass filters for dense wavelength division multiplexing," *Int. J. Adv. Appl. Sci.* **1**(2), 65–70 (2012).
6. T. Paatzsch, I. Smaglinski, and S. Krüger, "Compact optical multiplexers for LAN WDM," in *Plenary Meeting IEEE P802.3ba 40 Gb/s and 100 Gb/s Ethernet Task Force*, Denver (2008).
7. R. Nagarajan, "Fiber optic transmission engineering," *Proc. SPIE* short course SC133.
8. K. Okamoto, "Tutorial: fundamentals, technology and application of AWGs," in *24th European Conf. on Optical Communication (ECOC'98)*, Madrid, pp. 35–37 (1998).
9. W. Emkey, "Optical Transmission Systems and Equipment for WDM Networking," *Proc. SPIE* **4872**, 305–313 (2002).
10. D. Minoli, *Telecommunications Technology*, Artech House, Boston, London (2002).
11. M. K. Smit, "New focusing and dispersive planar component based on an optical phased array," *Electron. Lett.* **24**(7), 385–386 (1988).
12. A. R. Vellekoop and M. K. Smit, "Low-loss planar optical polarization splitter with small dimensions," *Electron. Lett.* **25**, 946–947 (1989).

13. A. R. Vellekoop and M. K. Smit, "A polarization independent planar wavelength demultiplexer with small dimensions," in *Proc. European Conf. Optics Integrated Systems*, Amsterdam, Netherlands, Paper D3 (1989).
14. A. R. Vellekoop and M. K. Smit, "Four-channel integrated-optic wavelength demultiplexer with weak polarization dependence," *J. Lightwave Technol.* **9**(3), 310–314 (1991).
15. M. K. Smit, "Optical phased arrays in integrated optics in silicon-based aluminum oxide," PhD Thesis, Delft University of Technology (1991).
16. H. Takahashi et al., "Arrayed-waveguide grating for wavelength division multi/demultiplexer with nanometer resolution," *Electron. Lett.* **26**(2), 87–88 (1990).
17. H. Takahashi, I. Nishi, and Y. Hibino, "10 GHz spacing optical frequency division multiplexer based on arrayed-waveguide grating," *Electron. Lett.* **28**(4), 380–382 (1992).
18. C. Dragone, "An N × N optical multiplexer using a planar arrangement of two star couplers," *IEEE Photonics Technol. Lett.* **3**, 812–815 (1991).
19. C. Dragone, C. A. Edwards, and R. C. Kistler, "Integrated optics N × N multiplexer on silicon," *IEEE Photonics Technol. Lett.* **3**, 896–899 (1991).
20. A. Kaneko et al., "Design and applications of silica-based planar lightwave circuits," *J. Sel. Top. Quantum Electron.* **5**(5), 1227–1236 (2002).
21. L. Eldada, "Optical add/drop multiplexing architecture for metro area networks," *SPIE Newsroom* (2008).
22. G. Y. Kim, "Simple and reliable bidirectional optical amplifier suitable for variable traffic pattern networks," *IEEE Photonics Technol. Lett.* **14**(4), 552–554 (2012).
23. H. Nishi et al., "Monolithic integration of a silica-based arrayed waveguide grating filter and silicon variable optical attenuators based on p-i-n carrier-injection structures," in *36th European Conf. and Exhibition on Optical Communication (ECOC)*, Torino, Italy (2010).
24. G. Keiser, *FTTX—Concepts and Applications*, IEEE Press, John Wiley and Sons, Inc., Hoboken, New Jersey (2006).
25. R. G. Broeke et al., "Optical-CDMA in InP," *IEEE J. Sel. Top. Quantum Electron.* **13**, 1497–1507 (2007).
26. G. Cincotti, "Optical signal processing using AWGs," in *40th European Conf. on Optical Communications (ECOC)*, Tu.4.6.1, pp. 1–3, IEEE, Cannes (2014).
27. M. K. Smit et al., "PHASAR-based WDM-devices: principles, design and applications," *J. Sel. Top. Quantum Electron.* **2**, 236–250 (1996).
28. M. K. Smit, "Progress in AWG design and technology," in *IEEE/LEOS Workshop on Fibers and Optical Passive Components*, Palermo, pp. 26–31 (2005).
29. Y. Hida, "400-channel arrayed-waveguide grating with 25 GHz spacing using 1.5%-Delta waveguides on 6-inch Si wafer," *Electron. Lett.* **37**, 576–577 (2001).
30. Y. Hida et al., "400-channel 25-GHz spacing arrayed-waveguide grating covering a full range of C- and L-bands," in *Proc. Opt. Fiber Communication Conf. Exhibition Technical Digest*, Vol. **3**, pp. WB2-1–WB2-3 (2001).
31. K. Okamoto, "Progress and technical challenge for planar waveguide devices: silica and silicon waveguides," *Laser Photonics Rev.* **6**, 14–23 (2012).
32. R. Adar, M. R. Serbin, and V. Mizrahi, "Less-than-1 dB per meter propagation loss of silica waveguides measured using a ring-resonator," *J. Lightwave Technol.* **12**(8), 1369–1372 (1994).
33. A. Sugita et al., "Very low insertion loss arrayed-waveguide grating with vertically tapered waveguides," *IEEE Photonics Technol. Lett.* **12**(9), 1180–1182 (2000).
34. S. T. S. Cheung et al., "Low-loss and high contrast silicon-on-insulator (SOI) arrayed waveguide grating," in *Proc. Conf. Lasers Electro-Optics*, pp. 1–2 (2012).
35. W. Bogaerts et al., "Silicon-on-insulator spectral filters fabricated with CMOS technology," *IEEE J. Sel. Top. Quantum Electron.* **16**(1), 33–44 (2010).

36. D. Dai et al., "Experimental demonstration of an ultracompact Si-nanowire-based reflective arrayed-waveguide grating (de)multiplexer with photonic crystal reflectors," *Opt. Lett.* **35**(15), 2594–2596 (2010).
37. T. Fukazawa, F. Ohno, and T. Baba, "Very compact arrayed-waveguide grating demultiplexer using Si photonic wire waveguides," *Jpn. J. Appl. Phys. II Lett. Exp. Lett.* **43**, L673–L675 (2004).
38. F. M. Soares et al., "Monolithically integrated InP wafer-scale 100-channel times 10-GHz AWG and Michelson interferometers for 1-THz-bandwidth optical arbitrary waveform generation," in *Proc. 2010 Conf. Optical Fiber Communication, Collocated National Fiber Optic Engineers Conf.*, pp. 1–3 (2010).
39. W. Jiang et al., "5 GHz channel spacing InP-based 32-channel arrayed-waveguide grating," in *Proc. Conf. Optics Fiber Communication*, pp. 1–3 (2009).
40. F. M. Soares et al., "Monolithic InP 100-channel × 10-GHz device for optical arbitrary waveform generation," *IEEE Photonics J.* **3**(6), 975–985 (2011).
41. F. M. Soares et al., "20 GHz channel spacing InP-based arrayed waveguide grating," in *Proc. 33rd European Conf. Exhibition Optics Communication*, pp. 1–2 (2007).
42. Y. Bo et al., "Compact arrayed waveguide grating devices based on small SU-8 strip waveguides," *J. Lightwave Technol.* **29**(13), 2009–2014 (2011).
43. M. B. J. Diemeer et al., "Polymeric phased array wavelength multiplexer operating around 1550 nm," *Electron. Lett.* **32**(12), 1132–1133 (1996).
44. B. Yang et al., "Compact arrayed waveguide grating devices based on small SU-8 strip waveguides," *J. Lightwave Technol.* **29**(13), 2009–2014. https://www.osapublishing.org/jlt/abstract.cfm?uri=jlt-29-13-2009
45. D. Dai et al., "Low-loss Si_3N_4 arrayed-waveguide grating (de)multiplexer using nano-core optical waveguides," *Opt. Exp.* **19**, 14130–14136 (2011).
46. D. Martens et al., "Compact silicon nitride arrayed waveguide gratings for very near-infrared wavelengths," *IEEE Photonics Technol. Lett.* **27**, 137–140 (2015).
47. S. Pathak, S. Kuanping, and S. Y. B. Yoo, "Experimental demonstration of compact 16 channels, 50 GHz Si_3N_4 arrayed waveguide grating," in *Optical Fiber Communications Conf. and Exhibition (OFC)* (2015).
48. X. J. M. Leijtens, B. Kuhlow, and M. K. Smit, "Wavelength filters in fibre optics," in *Arrayed Waveguide Gratings*, Vol. **123**, pp. 125–187 (2006).
49. G. Reed and A. P. Knights, *Silicon Photonics—An Introduction*, Wiley, Chichester (2004).
50. L. Pavesi and D. J. Lockwood, Eds., *Silicon Photonics*, Springer, Berlin (2004).
51. A. P. Knights and P. E. Jessop, "Silicon waveguides for integrated optics," Chapter 6 in *Optical Waveguides: From Theory to Applied Technologies*, M. L. Calvo and V. Lakshminarayanan, Eds., p. 231–270, CRC Press, London (2007).
52. P. Cheben, "Wavelength dispersive planar waveguide devices: echelle gratings and arrayed waveguide gratings," Chapter 5 in *Optical Waveguides: From Theory to Applied Technologies*, M. L. Calvo and V. Lakshminarayanan, Eds., pp. 173–230, CRC Press, London (2007).
53. S. H. Kong et al., "Integrated silicon microspectrometer," *IEEE Instrum. Meas. Mag.* **4**, 34–38 (2001).
54. J. T. Bradshaw, S. B. Mendes, and S. S. Saavedra, "Planar integrated optical waveguide spectroscopy," *Anal. Chem.* **77**, 28A–36A (2005).
55. Y. Deng, Y. Liu, and D. Gao, "Low crosstalk arrayed waveguide grating with cascaded waveguide grating filter," *J. Phys. Conf. Ser.* **276**, 012055 (2011).
56. K. Lee et al., "Effect of size and roughness on light transmission in a Si/SiO_2 waveguide: experiments and model," *Appl. Phys. Lett.* **77**, 1617–1619 (2000).

57. C. R. Doerr et al., "8-Channel $SiO_2/Si_3N_4/Si$/Ge CWDM receiver," *IEEE Photonics Technol. Lett.* **23**(17), 1041–1135.
58. C. R. Doerr et al., "Wide bandwidth silicon nitride grating coupler," *IEEE Photonics Technol. Lett.* **22**(19), 1461–1463 (2010).
59. K. Okamoto, *Fundamentals of Optical Waveguides*, Academic Press, New York (2000).
60. E. Wildermuth, "Performance optimization of flat-top passband arrayed waveguide grating demultiplexers," Dissertation ETH. Zürich, No. 13440 (1999).
61. H. Li et al., "Optimal design of an ultrasmall SOI-based 1 × 8 flat-top AWG by using an MMI," *Sci. World J.* **2013**, 636912 (2013).
62. Q. Fang, F. Li, and Y. Liu, "Compact SOI arrayed waveguide grating demultiplexer with broad spectral response," *Opt. Commun.* **258**(2), 155–158 (2006).
63. K. Maru and Y. Abe, "Low-loss, flat-passband and athermal arrayed-waveguide grating multi/demultiplexer," *Opt. Express* **15**(26), 18351–18356 (2007).
64. J. An et al., "Flat-top silica-based arrayed waveguide grating with 40-channels," *Optoelectron. Lett.* **2**(5), 323–325 (2006).
65. S. Pathak et al., "Optimized silicon AWG with flattened spectral response using an MMI aperture," *J. Lightwave Technol.* **31**(1), 87–93 (2013).
66. T. Saito et al., "Temperature-insensitive (athermal) AWG modules," *Furukawa Rev.* **24**, 29 (2003).
67. Photeon Technologies, http://www.photeon.com/company-history/ (2000).
68. T. Watanabe, S. Sohma, and S. Kamei, "Colorless optical add/drop using small matrix switch and cyclic AWG," in *18th Microoptics Conf. (MOC)*, Tokyo, p. 1–2 (2013).
69. http://www.ntt-electronics.com/en/products/photonics/colorless_awg.html.
70. http://www.neophotonics.com/_upload/pro/2010-09-19/1e0c0cbf-4908-4709-82e8-d95030356d93.pdf.
71. http://www.amstechnologies.com/fileadmin/amsmedia/downloads/8channel_50GHzArrayedWaveguideGrating.pdf.
72. http://www.enablence.com/media/mediamanager/pdf/8-enablence-datasheet-ocsd-awg-colorless-athermal-100ghzmultidemulti.pdf.
73. C. van Dam, "InP-based polarization independent wavelength demultiplexers," PhD Thesis, Delft University of Technology, Netherlands (1997).
74. Apollo Photonics, Inc., "APSS Apollo application note on array waveguide grating," http://www.apollophoton.com (February 2015).
75. Optiwave, http://optiwave.com/category/products/component-design/optibpm/ (February 2015).
76. N. K. Fontaine, R. P. Scott, and S. J. B. Yoo, "Dynamic optical arbitrary waveform generation and detection in InP photonic integrated circuits for Tb/s optical communications," *Opt. Commun.* **284**, 3693–3705 (2011).
77. Y. Chu et al., "The impact of phase errors on arrayed waveguide gratings," *IEEE J. Sel. Top. Quantum Electron.* **8**(6), 1122–1129 (2002).
78. N. Ismail et al., "Improved arrayed-waveguide-grating layout avoiding systematic phase errors," *Opt. Express* **19**(9), 8781–8794 (2011).
79. K. Okamoto, "Functional PLC devices for optical-layer signal processing," in *28th European Conf. on Optical Communication (ECOC 2002)*, **2**, pp. 1–19, IEEE, Copenhagen (2002).
80. D. Seyringer, M. Bielik, and M. Kytka, "Introduction of a new software tool to design arrayed waveguide gratings," in *Proc. APCOM*, Nový Smokovec, High Tatras, Slovakia, p. 122 (2011).
81. D. Seyringer and M. Bielik, "AWG-parameters: new software tool to design arrayed waveguide gratings," *Proc. SPIE* **8627**, 862716 (2013).
82. W. A. Shurcliff, *Polarized Light: Production and Use*, Harvard University Press, Cambridge, Massachusetts (1966).

83. D. Derickson, *Fiber Optic Test and Measurement*, Prentice Hall, Upper Saddle River, New Jersey (1998).
84. R-Soft, https://optics.synopsys.com/rsoft/rsoft-products.html (February 2015).
85. A. Rahman, "AWG-characterization," arphotonics.net (2001).
86. D. Seyringer and P. Schmid, "A new software tool is developed to evaluate the measured/simulated transmission characteristics of optical multilexers/demultiplexers," *Proc. SPIE* **8167**, 81671D (2011).
87. P. Schmid, "Development of a software tool to evaluate simulated and measured transmission characteristics of optical multiplexers/demultiplexers based on arrayed waveguide gratings," Master Thesis, FHV Dornbirn, Austria (2011).
88. International Laser Center, Bratislava, Slovakia, http://www.ilc.sk/en/vyskum/laboratoria/laboratorium-informacnych-technologii/ (February, 2015).
89. http://www.ntt-electronics.com/en/products/photonics/pdf/athermal.pdf.
90. https://www.oplink.com/pdf/AAWG-S0312.pdf.
91. K. Maru and Y. Abe, "Low-loss, flat-passband and athermal arrayed waveguide grating multi/demultiplexer," *Opt. Express* **15**(26), 18351 (2007).
92. L. Wang et al., "Athermal arrayed waveguide gratings in silicon-on-insulator by overlaying a polymer cladding on narrowed arrayed waveguides," *Appl. Opt.* **51**(9), 1251 (2012).
93. X. Wang et al., "Athermal silicon arrayed waveguide grating with polymer-filled slot structure," *Opt. Commun.* **282**, 2841–2844 (2009).
94. J. Chovan et al., "Temperature characterization of passive optical components for WDM-PON FTTx," *Adv. Electr. Electron. Eng.* **2**, 143–149 (2011).
95. D. Seyringer, "AWG optical demultiplexers: from design to chip, APCOM 2013," in *Proc. of APCOM*, High Tatras, Slovakia, p. 15 (2013).
96. D. Seyringer et al., "Design, simulation and evaluation of AWG based demultiplexers," in *IEEE Int. Conf. on Advanced Semiconductor Devices & Microsystems (ASDAM)*, Smolenice (Slovakia) (2012).
97. J. Nurjuliana et al., "Optimal design of linear tapered double S-shaped arrayed waveguide grating for broad channel spacing on silicon-on-insulator," *Opt. Eng.* **53**, 087110 (2014).
98. D. Seyringer et al., "Design, simulation, evaluation, and technological verification of arrayed waveguide gratings," *Opt. Eng.* **53**(7), 071803 (2014).
99. M. R. Amersfoort et al., "Passband broadening of integrated arrayed waveguide filters using multimode interference couplers," *Electron. Lett.* **32**(5), 449–450 (1996).
100. K. Okamoto and A. Sugita, "Flat spectral response arrayed-waveguide grating multiplexer with parabolic waveguide horns," *Electron. Lett.* **32**(18), 1661–1662 (1996).
101. C. Dragone, "Frequency routing device having a wide and substantially flat passband," U.S. Patent No. 5,412,744 (1995).
102. Y. P. Ho, H. Li, and Y. J. Chen, "Flat channel-passband-wavelength multiplexing and demultiplexing devices by multiple-Rowland-circle design," *IEEE Photonics Technol. Lett.* **9**(3), 342–344 (1997).
103. A. Rigny, A. Bruno, and H. Sik, "Multigrating method for flattened spectral response wavelength multi demultiplexer," *Electron. Lett.* **33**(20), 1701–1702 (1997).
104. K. Okamoto, K. Takiguchi, and Y. Ohmori, "Eight-channel flat spectral response arrayed-waveguide multiplexer with asymmetrical Mach–Zehnder filters," *IEEE Photonics Technol. Lett.* **8**(3), 373–374 (1996).
105. M. R. Amersfoort et al., "Phased-array wavelength demultiplexer with flattened spectral response," *Electron. Lett.* **30**(4), 300–302 (1994).
106. D. Seyringer, "Application of AWG-parameters tool in design of colorless 8-channel, 100 GHz AWG," in *Proc. of ICTON*, Cartagena, Spain, TU.p.16 (2013).

107. D. Seyringer, "Optisches Wellenleiterarray und optischer Wellenlängenmultiplexer/demultiplexer," Patent No. DE102,006,028,684 (B4).
108. Y. Hibino, "Recent advances in high-density and large-scale AWG multi/demultiplexers with higher index-contrast silica-based PLCs," *J. Sel. Top. Quantum Electron.* **8**, 1090–1101 (2002).
109. K. Takada et al., "12.5 GHz spaced 1.28 Tb/s (512-channel × 2.5 Gb/s) super-dense WDM transmission over 320 km SMF using multiwavelength generation technique," in *Proc. ECOC'00* (2000).
110. Y. Hida, "Recent progress on arrayed-waveguide grating wavelength multiplexer," *Proc. SPIE* **5595**, 339 (2004).
111. D. Seyringer, "Design and simulation of 128-channel 10 GHz AWG for ultra-dense wavelength division multiplexing," in *Int. Conf. on Transparent Optical Networks (ICTON 2012)*, Warwick, UK (2012).
112. D. Seyringer, "Improvement of the channel crosstalk in narrow channel spacing arrayed waveguide gratings applying specially shaped couplers," *Proc. SPIE* **7719**, 771923 (2010).

Dana Seyringer received her first Ph.D. in microelectronics at Slovak University of Technology in Bratislava in 1996 and her second Ph.D. at the JK University in Linz, Austria, in 1998.

In 2000 she joined the Austrian-based optical-chip-design company Photeon Technologies at the position of R&D Manager where she focused on the design of AWG based DWDM and CWDM multiplexer/demultiplexers along with other passive optical devices. She was instrumental in developing the company's special design methodology and design tools that allow high-quality AWGs to be designed in a very short time. In 2008, she joined the Research Centre for Microtechnology at Vorarlberg University of Applied Sciences in Dornbirn. She is internationally known for her work on simulation methods and is the author of numerous papers in the field of crystal growth and passive optical components for telecommunications.